Deanship of Graduate Studies

Al-Quds University

Liver Biopsy Sampling System Guided by the Internal Organs Motion and Ultrasound Imaging

Laila Ahmad Omar Abbasi

M.Sc. Thesis

Jerusalem-Palestine

1441 / 2020

Liver Biopsy Sampling System Guided by The Internal Organs Motion and Ultrasound Image

Prepared By:

Laila Ahmad Omar Abbasi

B.Sc.: Information Technology – Al-Quds University – Palestine

Supervisor: Dr. Radwan Qasrawi

A Thesis Submitted in Partial Fulfillment of Requirements for The Degree of Master in Computer Science / Department of Computer Science / Faculty of Graduate Students / Deanship of Graduate Studies / Al-Quds University.

1441 / 2020

Deanship of Graduate Studies

Al-Quds University

Computer Science

Thesis Approval

Liver Biopsy Sampling System Guided by The Internal Organs Motion and Ultrasound Image

Prepared By: Laila Ahmad Omar Abbasi

Registration No: 21720279

Supervisor: Dr. Radwan Qasrawi

Master thesis submitted and accepted, Date:

1- Head of Committee: Dr. Radwan Qasrawi Signature ...
2- Internal Examiner: Dr. Raed Zaghal Signature .....
3- External Examiner: Dr. Mohammad Hjouj Signature

Jerusalem – Palestine

1441 / 2020

Dedication

إلى الروح التي ما زالت دعواتها تحيطني وتملأني بالسكينة .. إلى من زرعت فيّ الطموح والشغف .. إلى روح جدتي الباقي دفئ قلبها حولنا.

إلى المعلّم والأستاذ الأول .. لمثال الصبر والحكمة .. إلى البسمة التي لن تنطوي ذكراها .. إلى جدّي – رحمه الله –

إلى العطاء المستمر .. إلى الداعم الأكبر والسند الدائم .. إلى من أفخر بكوني امتداداً لهما، إلى والديّ.

إليهم جميعاً .. أهدي هذا البحث.

Laila Ahmad Omar Abbasi

Declaration

I certify that this thesis submitted for the degree of Master, is the result of my research, except where otherwise acknowledged, and that this study (or any part of the same) has not been submitted for a higher degree to any other university or institution.

Signed: 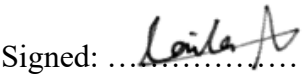

Laila Ahmad Omar Abbasi

Date: 22/08/2020

Acknowledgment

Foremost, I would like to express my sincere gratitude to my advisor Dr. Radwan Qasrawi for the continuous support of my thesis research, for his patience, motivation, enthusiasm, and immense knowledge.

I would also like to thank my thesis committee, Dr. Raed Zaghal, and Dr. Mohammad Hjouj for the insightful comments and feedback.

Finally, I must express my very profound gratitude to my parents and family for providing me with unfailing support and continuous encouragement. This accomplishment would not have been possible without them.

Abstract

Percutaneous needle access is a critical step of many clinical procedures, such as injections, diagnostic biopsies, and cancer ablation treatments, the higher the accuracy of needle placement and trajectory planning, the better the procedure results. However, the desired optimal needle targeting and positioning are challenging due to physiological respiratory motion and tissue deformation, which can cause mistargeting, resulting in needle placement error, ineffective delivery of treatment, or mistaken diagnosis. Advancement in medical technology and the development of image-guided navigation systems enable better interventional processes and higher procedure accuracy and efficacy. However, despite the wide variety of strategies and technologies implemented in needle placement and navigation systems, clinically applicable solutions are still lacking due to incompetent systems of addressing all technical and patient-specific challenges associated with image guidance interventions. The literature discussed the major effect of respiration on organs movement, and reported a high magnitude of organ displacement during breathing, specifying the organ motion as a major source of lesion targeting error in needle interventions. Although, the state-of-art image-guided navigation systems are not capable of compensating and dealing with this error factor.

The development of a precision image-guided navigation system that accounts for respiratory induced lesion displacement, integrated with medical imaging processing and computer vision techniques is proposed in this thesis. Aiming to control needle placement sources of error in clinical applications of biopsy sampling in a process that adapt to the current clinic workflow. The system provides physicians with preoperative feedback on needle biopsy sampling plan, allows for patient-specific biopsy plan, target tracking, performs image processing, volume rendering of targets region of interest, needle insertion, and extraction considering organ movement.

The system implemented MOSSE tracker for target region tracking during the intervention, and has been evaluated on 9 patients' data with 27 simulated liver tumor biopsy sampling procedures, and showed a reliable tracking with a high system accuracy with a mean overall

error of 1.78 ± 0.8 mm. The results show that controlling needle insertion based on the motion improved the targeting accuracy and made possible for future critical clinical applications.

Table of Contents

List of Tables

List of Figures

Definitions

ROI:	Regions of interest are the important and meaningful regions in the image. Regions of interest in medical images always are the focus regions such as tumors and calcified spots.[1]
GTV (Gross Tumor Volume):	The gross demonstrable location and extent of the tumor.[2]
CTV (Clinical Target Volume):	The CTV contains the demonstrable GTV plus a margin for sub-clinical disease spread. [2]
PTV (Planning Target Volume):	The geometric concept is designed to ensure that the radiotherapy prescription doses actual delivery to the CTV.[2]
OAR (Organs at Risk):	Also known as critical structures, are anatomical structures with important functional properties located in the vicinity of the target volume.[3]
DICOM:	Digital Imaging and Communications in Medicine DICOM Standard, specifies a non-proprietary data interchange protocol, digital image format, and file structure for biomedical images and image-related information.[4]
Motion Threshold:	Region of interest maximum amount of displacement (shift distance) allowed for needle insertion during the biopsy sampling procedure.
Seeding Point:	The center point of the region of interest.
Insertion Point:	The starting position of the needle on the skin surface for insertion.
Needle Path:	The distance between seeding and insertion points.

Chapter 1: Introduction

1.1 Introduction

Percutaneous needle interventions have been widely used as minimally invasive surgeries, that support multiple applications either diagnostic or treatment purposes, such as injections, diagnostic biopsies, and cancer ablation treatments. In such procedures, needle access is a critical step as the procedure success highly relies on the precision of needle insertion and targeting. The higher the accuracy of needle placement and less needle misplacement the better the procedure results.[5]

The standard clinical freehand approach in these procedures, cannot assure the required needle targeting precision since it's highly dependent on the operator experience [6] and lacks visual feedback and patient to image registration. This approach has drawbacks that minimize the efficiency and reliability of the procedure and can potentially cause side effects and complications.

The application of image guidance techniques and navigation technologies in percutaneous interventions are used and utilized to improve the accuracy and precision of these clinical procedures over the standard basic approaches.

Different medical imaging techniques are the key roles of image-guided procedures that provide either static or real-time patient-specific imaging information used for planning, guiding, and evaluation. With the advent of technology and medical image processing techniques, multiple studies have focused on developing computer-assisted navigation systems which are tools designed to facilitate target visibility and better lesion detection on an imaging modality and increase the ability to access the target precisely. [7]

The main components and functionalities of navigation systems include planning the procedure on image data, registration by matching of reference data set and working data set, tracking and localization of the instrument, visualization, and providing feedback.[7] Robotic

devices for percutaneous procedures can additionally provide physical needle placement and insertion and automatization of the intervention.[8]

However, these solutions are still not fully capable of overcoming procedures limitations and challenges. The efficacy of image-guided navigation systems relies on the accuracy of needle placement within a target lesion [9], and one of the major challenges in image guidance navigation systems is organs motion during respiration. The desired optimal needle targeting and positioning are still challenging due to respiratory motion and target displacement, which can cause mistargeting, resulting in an ineffective delivery of treatment or mistaken diagnosis.

The development of an image-guided needle navigation system that incorporates a method to compensate target motion error factors on needle targeting accuracy and provides a tool for preoperative biopsy procedure planning, and intraoperative feedback on needle insertion, relying on organ motion tracking and controlled insertion of the needle during the biopsy sampling, would be an added value to achieve higher precision of needle positioning at the planned target tissue.

1.2 Problem Statement

Percutaneous approaches have emerged in minimally invasive surgeries where access to inner organs or other tissue is done via needle puncture of the skin. Image-guided percutaneous approaches are increasingly used in interventional procedures for pre-procedural planning, needle targeting, intra-procedural treatment, and post-procedural assessment.

A manual freehand approach is conventionally employed during these procedures using a step-by-step technique where the physician mentally maps and registers the patient anatomy from the acquired images to insert the needle according to the planned trajectory. Due to the lack of actual real-time visualization feedback, estimating the target position and the required needle adjustment and orientation evaluation in each step requires image scan acquisition to assure accurate needle navigation along the path.

Multiple disadvantages arise from the iterative manner of this approach which leads to tissue damage with accompanying risks, increased procedure time and cost, patient and physician

excessive radiation exposure if the guiding modality utilizes ionizing radiation. Also, the performance of this method is highly dependent on the physician's skills and experience.

Achieving precise positioning of the tooltip at the predefined target tissue in biopsy operations is critical for interventional success but still challenging due to several patient-specific and technical parameters including 1) clarity of target determined by the lesion characteristics. 2) accessibility and visibility of needle trajectory avoiding critical structures and body organs. 3) the depth and angle of the needle path. 4) tissue motion and deformation caused by external forces, patient respiratory function, and body movement which increase the procedural complexity further.

The work presented in this thesis aims to overcome the above-mentioned challenges.

1.3 Research Questions

1. Does controlling needle insertion by organ motion tracking decrease the biopsy sampling error?
2. Is respiratory induced organ motion an important factor that shouldn’t be neglected during percutaneous interventions?
3. Does using CT-Ultrasound image registration in the needle navigation systems improve the biopsy sampling performance?

1.4 Research Hypothesis

According to the literature, as will be discussed later in Chapter 2, abdominal organs significantly move under influence of the respiration, and pulsation, causing the target lesion to displace resulting mistargeting and reduce the required accuracy in biopsy sampling.

By studying the motion factor, and the fact of the major effect it produces on procedures efficacy and accuracy, the research hypothesis states that ultrasound image-guided interventions improved and combined with control over insertion parameters (angle, depth, target distance) and considering the effect of respiration-induced motion on the needle

guidance by target tracking is sufficient to ensure the required targeting accuracy and procedural success in biopsy sampling.

1.5 Objectives of the Study

This thesis investigates methods and techniques to address the problems related to the current clinical approach. Focusing on the problem of respiratory induced organ motion during procedures, and considering an applicable solution that corresponds to clinical workflow and improves the procedure efficacy.

The purpose of this research is to develop a medical navigation clinical applicable system for biopsy sampling procedures guided by ultrasound imaging modality, and assess the needle target accuracy with a proposed algorithm considering organ motion-based needle adjustment.

Target lesion motion is not accounted for or considered in several approaches and image-guided navigation systems design. The main study objective is to explore and propose a method to encompass respiration-induced displacement of organs and eliminate needle targeting errors by controlling technical factors of planning parameters and target motion tracking which could increase the clinical applicability and target accuracy of needle interventions.

The specific thesis objectives can be summarized in the following points:

1. Develop a reliable and dynamic biopsy path planning simulator that decreases the risk of injuries and avoid organs at risk.
2. Examine potential methods and technologies that could help in reducing the effect of respiration-induced target motion on needle insertion efficacy.
3. Decrease the sampling error by developing an automatic needle insertion algorithm controlled by organ motion.
4. Enhance the ultrasound-guided biopsy sampling performance.
5. Ensure a clinical applicability and workflow adaptation of the proposed design.

1.6 Research Significance

Despite the number of image-guided navigation systems prototypes proposed and the different techniques and image modalities used, image-guided interventions still lack effective accurate clinical solutions, (Hodel et al., 2018) research experiment conducted to examine CT-guided biopsy sampling errors in chondrosarcomas and showed a high biopsy sampling error occurred in a total of ten patients (14.7%).[10]

The target lesion movement during respiration is a challenging factor that may result in needle targeting errors and critical structures damage. The majority of trajectory guidance systems are based on the assumption that the target lesion does not deform or displace by performing procedures under anesthesia or sedation and ventilation control methods. This assumption reduces the feasibility of several needle guidance systems.

(Hata et al., 2016)[11] confirmed the huge effect of organ motion on needle procedures efficacy. The authors have proposed a robotic instrument guide for orienting cryotherapy probes in image-guided cryotherapy of renal cancers and compared the accuracy between 60 insertions, half of them performed by the proposed robotic guidance, and the other 30 insertions were performed by operators with the freehand approach.

Hata study [11] shows that the robotic system accuracy results outstand the freehand insertion without introducing any motion, however, this advantage didn't exist anymore when target motion was introduced. The accuracy between the robotic 6.0 ± 3.1 and free-hand 5.9 ± 3.2 approaches becomes comparable when organ motion is present. Although, insertions performed with robotic guidance with no motion achieved a mean accuracy of 2.1 ± 1.3 and 6.6 ± 3.1 freehand.[11] These results show that organ motion source of error should not be neglectable and affect substantially on the procedure accuracy.

Precise needle positioning according to path planning is a prominent opportunity to develop assistance and navigation technologies to improve the efficiency and effectiveness of biopsy sampling procedure by providing motion tracking and needle placement feedback during the procedure.

1.7 Thesis Contribution

1. Developing a new method to encompass the effect of respiration induced target motion on needle insertion efficacy.
2. Providing image-based organ motion tracking during biopsy sampling.
3. Controlled needle insertion and adjustment by target displacement.
4. Preprocedural planning tool, intraprocedural feedback, and post-procedural accuracy assessment.

1.8 Research Methodology

The navigation system sampling-planning prototype is a medical image-based software to reduce biopsy sampling error in clinical settings. The software is a cross-platform operating system developed in C++ programming language, based on Medical Imaging Interaction Toolkit (MITK) open-source package and utilizing the OpenCV library.

The proposed solution uses medical ultrasound imaging for organ tracking and to continuously estimate the needle tip position about the previously planned needle path structure and target lesion. In addition to the US modality, computed tomography CT images are employed for defining and setting the sampling planning.

The system experiment was conducted on samples of liver ultrasound images sequence during breathing for 9 volunteers. Different clinical procedure plans and cases have been implemented with an expert radiologist help. Depth, shift, and overall error were the main parameters considered to assess and validate the proposed system accuracy.

The overall process can be divided into 3 main steps:

1. **Planning algorithms**

   A set of image segmentation and registration algorithms are integrated into the system for the planning step. Where an interactive segmentation tool is used for target lesion volume identification on CT data, and registration is performed aligning ultrasound

and CT images. In the planning phase, the user sets and plans the procedure parameters interactively, a tool is provided for the operator to set the needle tip-position for dynamically establishing the path between the target and insertion points. The system allows physicians to manipulate the needle path to find the best entry point ensuring avoidance of critical structures and tissue-damaging.

2. **Motion tracking algorithm**

   Completing the planning step, the procedure starts with tracking the target lesion based on the ultrasound series, controlling the insertion process, and providing the user with error calculations and feedback based on tracking results. For minimizing the sampling error and decreasing the missing sampling due to organ motion, a motion tracking algorithm is implemented for detecting the organ motion from the ultrasound images and providing controlled guidance based on the region of interest (ROI) position. Then the system continually calculates the sampling errors from the motion data, controlling needle insertion.

3. **Accuracy and error control**

   With the end of the insertion process, different error factors calculations are visualized for operators to assess the accuracy of needle targeting.

A detailed discussion of the methodology and the process phases will be explained further in Chapter 3.

1.9 Research Limitations

This research was conducted during the COVID-19 pandemic, which has interrupted our normal academic activities and made it very challenging at different levels.

Data collection was majorly affected, obtaining the data for the experiment was difficult, we couldn’t get any images from the local medical clinics at that time, so we had to shift to online options. Unfortunately, they were limited and not enough for the requirements, and we were hardly able to get the primary dataset we need.

Also, we couldn't find data subjects with specific features like (age, sex, weight, health situation) and the data collected lacked metadata and descriptive parameters about the volunteers, in addition to lack of clarity in some of the obtained ultrasound and CT images, which increased complications of dealing with the data.

The methodology was altered based on the availability and accessibility to the tools and devices needed. The solution was planned to be integrated with a robotic arm, to achieve an automatic dynamic needle insertion process. Also, organ motion was planned to be captured from a real-time ultrasound device. However, due to the lockdown situation, we weren't able to reach the university labs to work on the hardware connection of these devices.

1.10 Thesis Organization

Chapter 1 presents a general introduction to the research topic, problem discussion, formulating objectives, defining research questions, and hypotheses and declaring the motivation and contribution of the research.

Chapter 2, begins by proving a background of related topics in image processing, navigation systems, biopsy sampling procedures, and the study of organ motion. Then it presents an analysis and review of the state-of-the-art image guidance systems applied to percutaneous needle interventions, reporting their design, added values, and performance.

Chapter 3 first section describes the study design and data description, in the second section architecture, methodology, design, and workflow of the proposed system and the approaches followed in this thesis are discussed.

Experiments setup and results found are discussed and analyzed in Chapter 4.

Chapter 5, discusses the general findings and outcomes of this work and summarizes the thesis contribution in addition to presenting an outlook for potential future research.

Chapter 2: Background and Literature Review

2.1 Background

2.1.1 Medical Image Processing in Clinical Application

Medical images refer to the techniques and processes used to create images that allow for viewing the body internal parts for analysis, medical procedures, and visual representation. [12] Radiography, CT, MRI, and ultrasound are different available medical imaging modalities that are used in clinics for diagnosing and treatments by analyzing and studying the images information which is available digitally and can be processed efficiently and transferred with the help of communication networks and protocols such as Picture Archiving and Communication Systems (PACS) and the Digital Imaging and Communications in Medicine (DICOM) protocol.[13]

With the advancement in technology and its impact on the field of medical science, digital image processing techniques made it possible to be applied in clinical medical images to easily diagnose diseases and guide interventions. Image acquisition and forming as a digital image matrix, image enhancement and noise reduction, color correction, and edge detection [14] are major implemented techniques used for medical image processing to optimize the visual representation and help with initial pre-procedural steps such as organs identification and tumor detection.

Medical image processing applications are not only limited to pre-procedural steps, but it also has a major role during clinical procedures by providing image guidance and navigation systems that are increasingly rising, aiming to achieve better results and improve procedures quality. Medical imaging modalities, image manipulation, and instrument localization and tracking are the major common components of image guidance platforms.

- **Medical Imaging Modalities**

Different imaging modalities have been examined and utilized for intervention guidance, each has different characteristics, requirements, and purposes of use. Figure 2.1 shows an image instance for each modality.

- X-ray imaging

  X-ray is electromagnetic radiation that passes through the body, absorbed or attenuated at differing levels.[15] X-rays modality is widely used, it's quick, easily available, painless with low cost. It's typically used to evaluate and diagnose diseases and injuries, including broken bones, cavities, and tumors. However, X-ray is based on ionizing radiation which is harmful to the patient and increases the risk of developing cancer later in life.

- Computed Tomography (CT)

  CT is a volumetric image modality that combines multiple X-rays to produce images of cross-sections [14] that contain anatomical information providing a detailed view of the organs, bones, tissues, and blood vessels inside the body. CT is widely used for diagnosing diseases and more serious problems. It helps in planning and guiding interventional procedures such as biopsies. Also, can be used for assessing treatments and therapies. But still, CT scanners are based on ionizing radiation that is harmful to the patient and the physician and it lacks real-time information during procedures.

- Magnetic Resonance Imaging (MRI)

  A strong magnetic field and radio waves are using to produce medical images for the body structures using MRI scanning.[16] It also provides 3D image datasets and anatomical information, especially for soft tissues since it has good soft-tissue contrast. Commonly used to examine internal body structures, spinal injuries, and brain function. The one major advantage that MRI has over CT is that it does not emit any ionizing radiation, so it's much safer. However, it's expensive and takes a long time during the imaging process.

- Ultrasound

Using high-frequency sound waves, ultrasound image modality produces dynamic real-time images. Unlike X-ray and CT, it relies on waves rather than ionizing radiation, so it minimizes the radiation exposure related risks and provides a safe solution. Common applications of ultrasound in clinics are during pregnancy for baby checking, imaging for organs in the abdomen like liver and kidneys, also for breasts, muscles, and blood vessels.

Ultrasound is low-cost, when compared to CT and MRI, the spatial resolution in ultrasound is high.[17] It's also capable of providing real-time information with no radiation exposure. The drawback of the ultrasound is low image quality and low contrast resolution.

(a) X-Ray Image of human

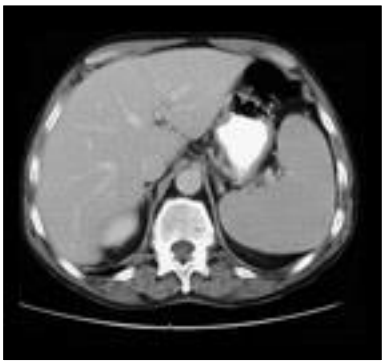

(b) Abdominal CT image

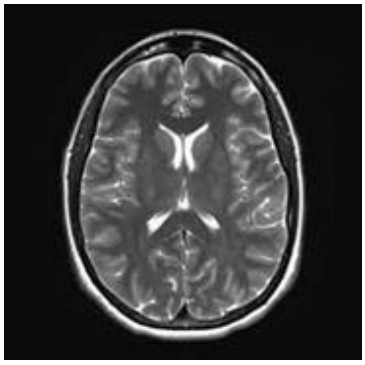

(c) MRI scan for the brain

(d) Ultrasound view of the liver and right kidney

Figure 2.1 Medical Images from different Medical Imaging Modalities

Among this variety of imaging modalities, there is no single suitable modality for all tissue structures and organs, each modality has it's own range of applications and provides different information. X-ray, for example, works more efficiently on hard tissues like bones, CT provides better images of soft tissue than X-rays, and both modalities are effective in assessing structural and morphological information. MRI has a high contrast between soft tissues such as muscles, cartilage, brain tissue, and blood vessels. Anatomical, functional, and cellular information can be provided by MRI. Ultrasound imaging can provide anatomical information, it can capture images of the pelvis and abdomen but molecular imaging agents issues limit the types of tissues that can be imaged. [18]

Multi-modal imaging approach can help to minimize and to overcome the drawbacks and limitations of individual image modalities, by combining and taking advantage of the desirable characteristics from different modalities.

- **Image Manipulation: Segmentation, Registration, and Fusion**

Different image manipulation and processing methods are utilized in image-guided navigation systems. Image segmentation can contribute to image-guided interventions by helping with identifying and highlighting lesions of interest and isolate them for analysis. It allows the operator to visualize body structures, processes simulation, pathologies localization, assessment, and evaluation.[19]

Image registration is another image processing technique applied on two or more medical images to achieve proper integration of useful data obtained from separate imaging modalities and for comparing different images. Also, images from different imaging modalities can be fused and aligned by image fusion techniques for the integrated display of these modalities.[20]

- **Localization and Tracking**

Information about the instrument position and orientation relative to the target region is primarily needed during minimally invasive interventions, to be able to make decisions and evaluate the process efficacy. Image-guided navigation systems implement different tracking strategies and technologies. Tracking devices can be used to determine the position and orientation of a tracked tool, optical tracking uses cameras to capture and track light-reflecting markers attached to the instrument. Electromagnetic tracking systems are an alternative that uses an emitter to generate an electromagnetic field for instrument position detection.[21]

Image-based detection and pose estimation is another technique for tracking where the instruments can be tracked and estimated in the reference frame by extracting image features.[22]

The discussed three components (Image Modalities, Image Manipulation, and Localization) are the main integral elements of image-guided systems. To study image guidance in minimally invasive interventions, we will focus on percutaneous needle biopsy (PNB) as our case study which is clinically performed guided by imaging modalities such as ultrasound, CT, and MRI [23].

2.1.2 Biopsy Sampling (Liver Case Study)

The liver is the largest organ in the body, accounting for approximately 2% to 3% of average body weight. It's placed in the right upper quadrant of the abdominal cavity protected by the rib cage. [24] Liver biopsy is a procedure performed to acquire a tissue sample (specimen) for analysis and examination that helps in the diagnosis, staging, assessment, and assist with treatment options and clinical management of liver disease or disorders.[25] There are three main types of liver biopsy approaches 1) Percutaneous Liver Biopsy, 2) Transvenous Liver Biopsy, 3) Laparoscopic Liver Biopsy.[26]

Percutaneous liver biopsy is a common type of liver biopsies, where the operator inserts a needle through the skin in the abdomen into the liver and extracts a small piece of tissue. This approach is often applied using ultrasound imaging guidance.

The procedure using ultrasound image guidance as Albhaisi et. al [27] report it, starts with placing the patient in a supine position with their right arm behind their head. Then, using ultrasound, the optimal site for biopsy is localized. Followed by applying local anesthetic is to numb the area. Once the skin is anesthetized a small incision is made for the needle to be inserted between the ribs. At this moment, the patient is instructed to take a breath in, and breathe out, and then to hold their breath. While the patient is holding their breath, the needle is introduced into the liver monitored by image guidance.

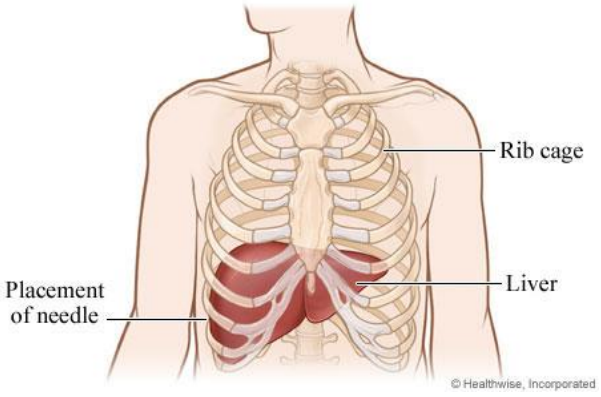

Figure 2.2: Placement of Liver Biopsy Needle

Figure 2.2 shows liver organ position in the human body and liver biopsy needle placement according to Healthwise clinical review. [28]

In liver biopsy procedures, the quality of the liver tissue and the sample size is important, biopsy samples should be representative to achieve accurate diagnosing and assessment.[29] Accomplishing that can be difficult due to normal surrounding tissues of the ROI and respiratory induced organ motion which not only affects the sample extraction quality but also the displacement of the needle due to these factors might cause damage and serious complications. The hepatic artery and portal vein are the most significant main blood vessels at risks that supply the liver [24] (as shown in Figure 2.3)[30]. Miss targeting and inadvertent perforation of the hepatic or portal vein or aberrant hepatic artery may cause death.[31]

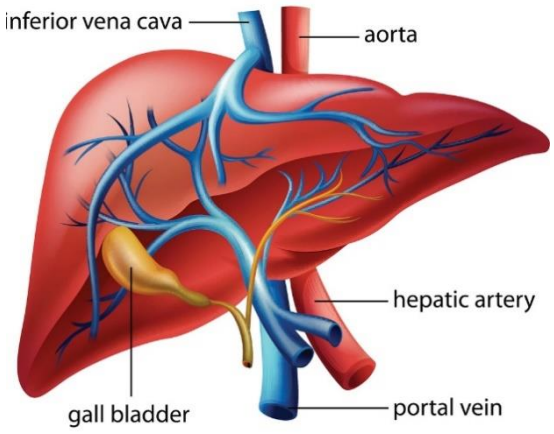

Figure 2.3: Hepatic artery and the portal vein in liver anatomy

Adverse effects may occur due to exposure to surrounding healthy tissues, injury, and damage to sensitive structures. As a consequence of organ motion, the needle may stick in another internal organ or healthy tissue during a liver

biopsy causing damage, bleeding, and injury or might lead to death due to the laceration in the liver if the biopsy needle is inside the liver while the patient deeply inhales.[31]

Multiple other potential complications may arise during and after biopsy, and it's proportional to clinician expertise and the number of biopsies taken. The most significant risk is bleeding, other risks include haemobilia, non-hepatic organ puncture, pain, infection, and reaction to the local anesthetic.[32] Also, (Subar, et al.) [33] reported death, septicemia (a result of bacteremia during needle biopsy), and perforation of nearby organs as immediate complications of liver biopsy.

An image-guided liver biopsy can still be challenging due to multiple factors including the location of the liver behind the rib cage and the need for careful needle insertion between the ribs, in addition to the nearness of surrounding vessels or organs and changing lesions positions and due to respiratory motion. [34]

2.1.3 Biopsy Sampling Error

Sampling error is defined as the deviation of a sample from the population (or tissue) from which it was taken. [35] Biopsy sampling error is often a result of inaccurate needle localization. [36] The overall targeting error in biopsy sampling can be broken down into target lesion shift error, and depth error as illustrated in Figure 2.4 [37], achieving minimal overall error, increase accurate needle placement and reduce mistargeting hence sampling error.

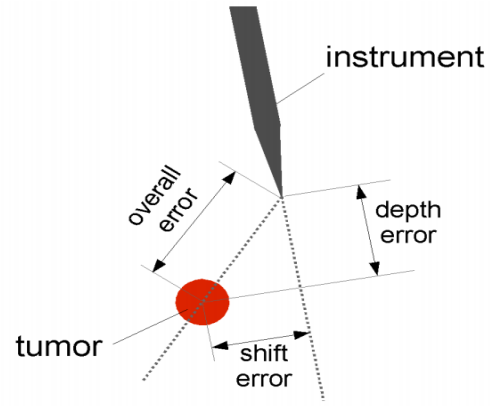

Figure 2.4: Illustration of the overall targeting error, the shift error, and the depth error

Studies reported a high sampling error rate in liver biopsy procedures. [10][38] Tissue obtained by biopsy needle is around one of 50,000 representing a tiny part of the liver mass, which increases the possibility of sampling error in a liver biopsy.[35]

Another complicating challenging factor causing sampling error is respiratory organ motion. Liver displacement and movement during breathing introduces a significant amount of uncertainty in locating the target lesion, the deviation between the intended and delivered needle targeting position for tissue sampling increases the intervention complexity and contributes to a high rate of sampling errors. In such cases, the sample of liver tissue is not representative and does not reflect the tissue situation for an accurate diagnosis.

To find the current challenges in needle placement and reasons behind needle placement errors a questionnaire was administered at the Annual Meeting of Cardiovascular and Interventional Radiology Society of Europe in 2016 by (de Jong et.al. [39]). The questionnaire was filled by 135 expert subjects, the majority were radiologists with experience in needle placement.

Multiple technical and patient factors have been identified as challenges in needle placement. Needle bending and deflection inside the tissue, poor needle visibility, and limited imaging possibilities were addressed as the technical factors. Respiratory induced Movement of the target, critical structures as vessels near the target, and movement of the target upon needle insertion were mentioned as patient-specific challenging factors. The questionnaire results show that 90% of the respondents strongly agree that the target hitting is complicated and needle displacement occurs because of respiratory induced target motion.[39]

As can be seen, liver motion due respiratory is a major factor that should be considered to achieve an accurate needle placement and lesion targeting, hence minimizing biopsy sampling error attaining a successful safe biopsy procedure.

2.1.4 Respiratory and Organs Motion

Oxygen represents the basic element that our bodies need to survive. The process of which we exchange gases with the environment by bringing in oxygen-rich air into the lungs and flushing out carbon dioxide in return is called respiration. The respiration process consists of two phases, inspiration, and expiration, oxygen is taken into the lungs by inspiration, and carbon dioxide is evicted from the lungs by expiration.

The contraction and relaxation of muscles change the volume of the thoracic cavity, resulting in changing the volume and the pressure inside the lungs. The diaphragm is the primary

breathing muscle that moves upward and downward during respiration. During inspiration, the diaphragm contracts and moves down, and the abdomen is forced inferiorly and anteriorly. This increases the size of the thoracic cavity and decreases the pressure inside the lungs allowing the air to rush in and fill the lungs. During expiration, the diaphragm relaxes and moves up, and the volume of the thoracic cavity decreases, while the pressure in the lungs increases. As a result, the air is pushed out. Our inner organs lie under the diaphragm. So, when the diaphragm moves downward, it takes up space in the belly area by pushing down into the inner organs causing them to displace and shift. Organs located within and surrounding the thoracic and abdominal cavity such as lungs, liver, kidney, and pancreas move under the influence of the respiration.

The team from the Max Planck Institute for Biophysical Chemistry (MPIBC) in Germany has released footage that shows the motion of a person's internal organs as they breathe naturally.[40]
Figure 2.5 displays clips of the video showing the internal organs in the inspiration and expiration phases during breathing.

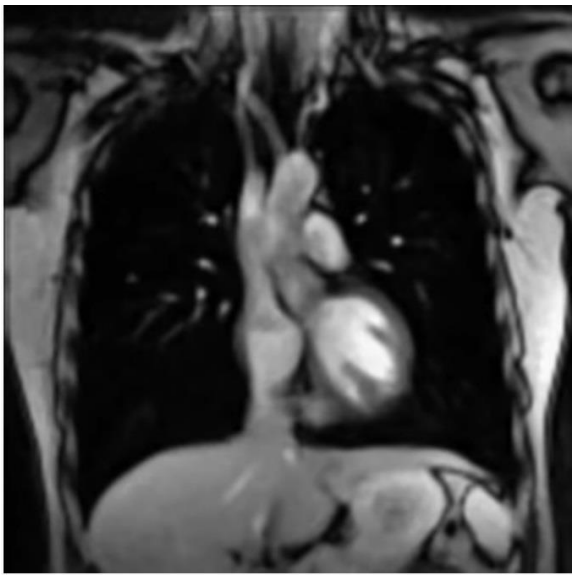

(a) Inspiration Phase

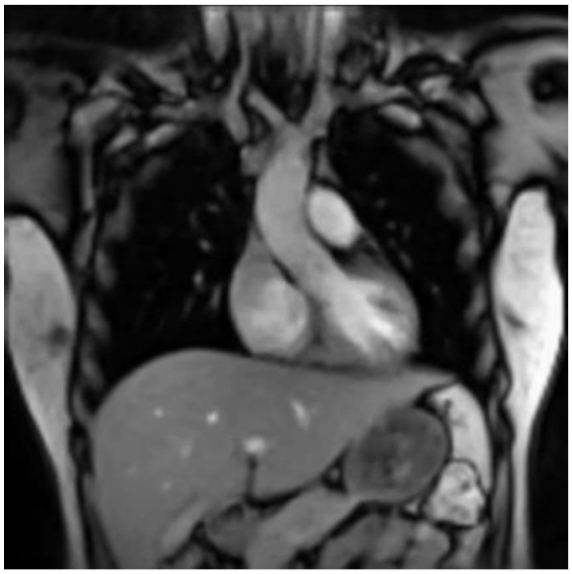

(b) Expiration Phase

Figure 2.5: Coronal MR images of Internal organs in inspiration and expiration phases

In the next sections will specifically discuss liver motion and different respiratory motion management techniques used in clinical interventions.

2.1.4.1 Liver Motion

Respiration induced motion magnitudes of body organs have no general patterns and vary according to different parameters and many individual characteristics of breathing like quiet versus deep, chest versus abdominal, healthy versus ailing.[41] Different studies have observed and described the magnitude of respiratory motion and the way organs deform and displace during respiration using different methods. Table 2.1 summarizes these studies and their findings regarding motion magnitude.

Bussels, et al. [42] assessed the effect of respiration on upper abdominal organs in 12 subjects using dynamic MRI. The pancreas and liver were the largest organ movements in cranio-caudal direction (23.7 ± 15.9 mm and 24.4 ± 16.4 mm). The liver movement in the coronal Y direction was 24.4 ± 16.4 mm. In the sagittal Y direction, the mean maximal movement was 17.5 ± 6.7 mm. Smaller movements were seen in the coronal X (LR) and sagittal X direction (AP): 13.2 ± 6.9 mm and 9.0 ± 3.5 mm

Davies, et al. [43] found that liver motion is predominantly in the superior-inferior (SI) direction with an average displacement of 10 ± 8 mm (range 5-17 mm) in quiet breathing and an average of 37 mm (range 21 – 57 mm) in deep breathing.

Suramo, et al. [44] examined liver motion in 28 patients. The study emphasizes that the liver proved to be the most movable organ in both normal respiration and standardized breathing. The range of liver movement in normal respiration is 10-40 mm and 30-80 mm in deep maximum respiration.

Using cine-MRI on 36 patients to measure the motion of liver tumors during free-breathing, Kirilova et al.[45] found that the average cranial-caudal tumor motion was 15.5 mm range between 6.9–35.4), anteroposterior motion was 10 mm and a range between 3.7–21.6

Suramo et al. stated that "The liver proved to be the most movable organ in both normal respiration and standardized breathing." [44] So, it's evident from the studies that liver organ motion cannot be ignorable and should be taken into account during percutaneous needle interventions.

Table 2.1: The mean and range of liver motion in Superior-Inferior (SI) / Cranio-Caudal (CC) direction in millimeters.

Study	Number of Subjects	Normal Respiration	Deep Respiration	Modality
Bussels	12	24.4 ± 16.4	-	MRI
Davies	9	10 ± 8 (5-17) mm	37 (21-57) mm	US
Suramo	28	25 (10-40) mm	55 (30-80) mm	US
Kirilova	36	15.5 (6.9-35.4) mm	-	MRI

2.1.4.2 Respiratory Motion Management Techniques

Abdominal body organ motion is majorly influenced by the respiratory and has shown relatively large shifting margins that affect needle intervention efficacy. Several methodologies for motion monitoring have been introduced for the sake of managing and encompassing organs induced respiratory motion. Some of the main approaches are discussed in this section.

Motion suppression methods involve controlled organs movement by breath-holding, abdominal pressure, and ventilation techniques. Breath-holding is a common technique where the intervention is performed at certain points in the breathing cycle, This method is simple but relies on the ability of the patient to cooperate, and the capability they can tolerate breath holds which may be limited and dependent on patient age, health situation, weight, and other factors.

Abdominal pressure is another approach where the organ motion is physically constrained by a compression device. The applied pressure to the abdomen reduces diaphragmatic movement and organ motion accordingly.

High-frequency ventilation (HFV) is mechanical ventilation uses small tidal volumes and rapid ventilator rates, High-frequency jet ventilation (HFJV) is one type of HFV, produced by ventilators providing high-velocity jet of gas directly into the airway [46] It releases short jets of gas in the inspiratory cycle decreasing the associated respiratory movement.
Another approach for motion compensation is respiratory gating. Gating techniques are more flexible, it doesn't require holding the breath for patients as they can breathe freely. Procedures with respiratory gating techniques progress only within a specific portion of the patient's breathing cycle called "gate" determined by monitoring the patient's respiratory motion, using fiducial markers.[41]. The patient respiratory motion can be monitored using external or internal markers. External tracking using infrared markers can be placed on the abdominal surface so that a motion sensor can measure the effect of respiratory motion on the liver. For higher accuracy, internal tracking can be done using fiducial markers implanted in the target volume to deliver motion estimation.

2.2 Literature Review

2.2.1 Medical Image Processing in Clinical Application

Different imaging technologies and image processing techniques play a major role in diagnostic and therapeutic clinical procedures resulting in better treatment and early disease diagnosing.

Multiple studies have focused on tumor detection using image processing techniques, (Murthyet et al., 2014)[47] describe a segmentation method using thresholding and morphological operation for brain tumor detection and feature extraction which is useful in clinical examination and treatment planning. (Devkota et al., 2018)[48] study proposed a segmentation algorithm to diagnose brain tumors in its early stage using Mathematical Morphological Reconstruction (MMR) with a 92% accuracy of cancer detection experiment result. Another brain tumor detection and segmentation method were proposed by (Rajan et

al., 2019)[49] on MRI image modality, by integrating K-means clustering with Fuzzy C-Means (KMFCM) and active contour by level set for tumor segmentation.

Liver tumor detection has also been studied in clinical applications, (M. Linguraru et al., 2012)[50] presented an automated technique to segment liver tumors from CT images with inconsistent enhancement and imaging artifact. (Wu, Xin'ai et al., 2016)[51] discussed detecting a serious cause of cancer death, the Primary Hepatic Carcinoma (PHC) tumor using different imaging methods (Ultrasound, CT, MRI, PET/CT) and showed that combining different modalities could greatly improve the detection rate of PHC.
In addition to the use of medical imaging techniques for diagnostic purpose, it's also utilized in the treatment and pretreatment process, (Tang et al., 2006)[52] proposed a method to improve the registration accuracy of MRI images which lacks clear target visualization and preoperative CT images in liver cancer treatment by applying affine registration followed by BSpline-based nonrigid registration. (H. Lu et al, 2016)[53] developed a liver image registration method for integrating the diagnostic pre-operative contrast-enhanced CT images and intra-operative non-contrast-enhanced CT images to improve image guidance liver ablation treatment intervention. (Chengxi Li, Andrew Zhu, 2020) [54] have presented the clinical application of image fusion technique and different algorithms in liver tumor diagnosis and treatment on different combinations of image modalities.

As the studies show, image processing techniques including segmentation, registration, and image fusion have been effectively employed in medical image processing for enhancing clinical interventions.

2.2.2 Needle Navigation Systems

Needle navigation systems have gained research focus to identify and apply methods in clinical interventions aiming to overcome needle interventions challenges and improve the process accuracy utilizing image guidance and navigation technologies.

This section presents an overview of needle navigation systems ranging from simple passive aids to active needle guidance robotic systems with different navigation and tracking methods.

Optical tracking systems are commonly used technique and widely adopted in interventions navigation, it uses cameras to capture and track light-reflecting markers attached to the instrument. Several markers are also attached to the patient's anatomy to enable registration with the acquired image data set concerning the tracking system. One of the main restrictions of optical tracking systems is requiring an unobstructed continuous line of sight between the camera and the markers which restrain instruments and staff placement and limit the workspace.

(Oliveira-Santos et al., 2011) [55] proposed an optical navigation system for percutaneous needle interventions based on PET/CT image modalities. Their work presents a multimodal approach combining structural (CT) and functional (PET) image modalities in order to enhance and optimize the diagnosis. The system consists of a computer, optical position sensor and dynamic reference (DR) set composed of a needle and patient dynamic references. The system tracks each DR and displays visual feedback. The proposed navigation system has been evaluated on swine cadavers and presented an average overall accuracy of 4.23mm for bone and 3.07mm for soft tissue punctures.

Important features of this system that it supports the clinically applicable workflow by considering clinical protocols and providing a workflow that integrates planning, calibration, and registration. It also focuses on bony lesions' challenges and provides a system for both soft tissue and bone punctures, and it minimizes radiation exposure since it requires only one image acquisition. However, it's designed to target static anatomical regions not taking into account the applicability of moving organs.

CAS-One, CAScination is a commercially available optical navigation system. **(**Engstrand et al., 2016) [56] study evaluated the accuracy and safety of antenna placement performed with a CT-guided CAS-One navigation system for percutaneous ablation of liver tumors. Patient to image registration and real-time tracking was achieved by attaching markers to the skin of the patient. High-frequency jet ventilation (HFJV) technique has been used to overcome liver movement due to respiratory. The results of ablations on 20 patients showed a total error of 5.8 ± 3.2 mm

(Chih Yu An et al.,2017) [57] developed an ultrasound imaging-guided robotic high-intensity focused ultrasound (HIFU) treatment system that integrates (ALOKA, Prosound Alpha 6) ultrasound imaging system, HIFU ablation system, a robotic arm, and the (Northern Digital, Polaris Spectra) optical tracker. During the process, the ultrasound probe movement is detected by the optical tracker through dynamic reference, the position of the tumor phantom relative to the ultrasound image gets transferred to the robot coordinate frame, so the robotic arm can move the focal point of the HIFU transducer for tumor ablation.

The system HIFU treatment experiment was conducted on four corner point ablation procedures on a phantom, the average distance error was 1.32 ± 0.58 mm. The study conclusion highlights the necessity of considering the path planning issue and the respiration problem.

(Yamada et al., 2020) [58] developed an MRI-US multi-modal image-guided navigation system for tumor ablation treatment. The system comprised a robotic arm needle manipulator with an ultrasound probe, an optical tracking sensor, MRI-compatible monitors, and a wide-bore MRI scanner. For accurate needle insertion, the insertion process was guided by real-time ultrasound imaging fused with the static MRI image. The developed system was evaluated on a phantom resulting in a targeting error for 50 insertions of 1.6 ± 0.6 mm.

A summary of these studies is provided in tables 2.2,2.3,2.4

Table 2.2: Summary of optical tracking navigation systems

Study	**Procedure**	**Image Modalities**	**Target**	**Experiment**
Oliveira-Santos	Punctures	CT/PET	Soft tissue and bone lesions in swine cadavers.	4 swine cadavers
Engstrand	Ablation	CT	Liver	28 tumors in 20 patients
Chih Yu An	Ablation	Ultrasound	Phantom	four corner points of a phantom
Yamada	Ablation	Ultrasound/MRI	Phantom	50 insertions on agar phantom

Table 2.3: Summary of optical tracking navigation systems accuracy - a

Study / System	Error Factors	Accuracy
Oliveira-Santos	Overall error: - The error introduced by a patient DR movement - Internal tissue deformation error - User-system error	Bone: 4.2 ± 2.0mm Soft tissues: 3.1 ± 1.2 mm
Engstrand / CAS-One	Mean lateral error: Normal distance between the planned trajectory and the antenna at the planned target position.	4.0 ± 2.5 mm

Table 2.4: Summary of optical tracking navigation systems accuracy - b

Study / System	Error Factors	Accuracy
Engstrand / CAS-One	Depth error: Longitudinal distance from the antenna tip to the target along the planned trajectory.	3.4 ± 3.2 mm
	Total error: Euclidean distance between the antenna tip position achieved and the planned target position.	5.8 ± 3.2 mm
Chih Yu An	Average distance error	1.32 ± 0.58 mm
Yamada	Targeting error	1.6 ± 0.6 mm

Table 2.5: Summary of optical tracking navigation systems time

Study / System	Time
Oliveira-Santos	The actual instrument guidance time during puncture averaged 7.5 min and 5.5 min for targets located in bone and soft tissue.

Engstrand / CAS-One	Median: 39.5 min

Electromagnetic based navigation systems are also available in intervention guidance, this method overcomes the line-of-sight restrictions of optical tracking.

IMACTIS® device (Imactis, Grenoble, France) is an electromagnetic navigation system. A magnetic field generator is placed near the needle entry site and an electromagnetic sensor is embedded in the needle holder. The system enables the physician to track and evaluate the needle trajectory by visualizing needle trajectory on static CT images. (Moncharmont, Moreau-Gaudry, Medici, & Bricault, 2015)[59] have investigated the performance of the IMACTIS robotic assistance during CT-guided procedures in a prospective, randomized, comparative phantoms study. The results demonstrate using IMACTIS system operators performed faster and more accurate phantom punctures (3.7mm) than the standard CT-guided method with (17mm) accuracy.

Also, (Durand et al., 2017) [60] reported an assessment of the accuracy of the IMACTIS electromagnetic navigation system in CT guided interventions and compared both traditional and navigated procedures.

The results of the procedures performed on 120 patients, also confirm that accuracy improved using the navigation system. But still one of the major drawbacks of this system is that the device cannot track respiratory motion, which causes the need to adopt a breath-hold approach during certain procedures to increase the accuracy of needle placement.

(Volpi et al., 2019)[61] discussed the limitations of accessing small or hard to spot lesions and the improvement of needle placement by the use of HFJV ventilation method to reduce respiratory movements of target organs. It evaluates the combination of computed electromagnetic navigation IMACTIS with HFJV for the ablation of small US-invisible liver tumors. After automatic HFJV was initiated CT scans of small tumors were transferred to the IMACTIS-CTVR navigation system, which is composed of a magnetic transmitter, a needle holder with an electromagnetic locator. Percutaneous ablation was performed in 21 patients with a mean tip to tumor distance of 22 ± 19 mm which is relatively high and a mean radiation dose of 558 mGy*cm.

(Putzer et al., 2016) [62] and his group have compared the targeting accuracy and reliability of electromagnetically guided punctures in a phantom model using two commercially available navigation systems (AxiEM and PercuNav). The experiment performed 480 total punctures with both navigation systems, 80 punctures each at three different slice thicknesses (1, 3, and 5mm).

For evaluation the deviations between the planned puncture trajectory and the actual needle path were evaluated, the Euclidean distance and the lateral positional error between the tip of the needle and the tip of the target were calculated.

Based on the results, AxiEM was more accurate comparing to PercuNav for CT with 3mm slice thickness. Possible interference with external magnetic fields may occur. Also, target movement including respiratory must be taken into account and compensated for in the clinical setting.

(Xiao et al., 2017)[63] compared the accuracy of a Kinect-optical and Veran IG4 electromagnetic navigation system for percutaneous liver needle intervention. The EM used marker-based registration. Kinect-Optical system registration is performed based on a surface-matching algorithm. Both navigation systems can compensate for respiratory motion based on real-time registration. 18 needle insertions on 5 beagles were performed using both the optical and EM navigation systems. The accuracy measured by the target positioning error (TPE) of the Veran IG4 system was 8.72 mm exceeds the accuracy of the Kinect- Optical system of 6.78 mm. Kinect-Optical system processing time was 10 mins, similar to that of the Veran IG4 system 12 mins.

A summary of these studies is provided in tables 2.5,2.6,2.7

Table 2.6: Summary of EM tracking navigation systems

Study	**Procedure**	**Medical Imaging Modalities**	**Experiment**
Moncharmont	Biopsy	CT	Phantom study with 2 targets (54 navigated and 54 freehand needle

			placements
Durand	drainage, biopsy, tumor ablation, infiltration, sympathicolysis	CT	120 patients
Volpi	Ablation	CT	Liver
Putzer	Punctures	CT	
Xiao	Ablation	CT	Liver

Table 2.7: Summary of EM tracking navigation systems accuracy

Study	**System**	**Error Factors**	**Accuracy**			
Monchar-mont	IMACTIS	Median distance to the center of the target	NAV: 3.7 mm vs. control: 15 mm			
Durand	IMACTIS	Distance Error	NAV = 4.1 CT = 8.9			
		Angle Error	NAV = 4.7° CT = 7.9°			
Volpi	IMACTIS	Mean path-tumor angle	7 ± 4 degrees			
		Mean tip-to-tumor distance	22 ± 19 mm			
Putzer	AxiEM	The Euclidean distance between the tip of the needle and the tip of the target. (mm)		1mm	3mm	5mm
			ED	3.86 ± 2.28	3.74 ± 2.1	4.81 ± 2.07
			LPE	3.29 ± 1.52	3.16 ± 1.52	3.93 ± 1.68
	PercuNav	The lateral positional	ED	4.42 ±	4.26 ±	4.46 ±

		error between the tip of the needle and the tip of the target. (mm)		1.33	1.32	1.56
			LPE	3.84 ± 1.59	3.84 ± 1.43	3.81 ± 1.71
Xiao	Kinect-optical	Distance from the needle tip to the planned tumor centroid	6.78 mm			
	Veran IG4		8.72 mm			

Table 2.8: Summary of EM tracking navigation systems time

Study / System	**Time**
Moncharmont / IMACTIS	nav: 01:16 min vs. control: 03:34 min
Volpi / IMACTIS	51 (23-108) min
Putzer / AxiEM	2 -5 min

Both technologies have main limitations, optical tracking requires a continuous line of sight, and electromagnetic devices can't be used on patients with non-electromagnetic-compatible devices or implanted material.

The systems discussed above only provide visual feedback about how to position the needle, and fully rely on the operator for the actual needle control actions. Unlike active needle guidance systems where physical guidance is during needle placement in order to minimize the user dependency and increase targeting accuracy. These systems can also be categorized based on mounting type: patient mounted and table-mounted.

Patient mounted systems are directly attached to the patient's skin, it enters the imaging field with the patient and captures the patient's movement providing better accurate targeting.

(Hungr, Bricault, Cinquin, & Fouard, 2016)[64] developed a patient mounted robotic system for procedures under CT and MRI guidance. The system is designed for the thorax and abdomen. For automatic registration, the robot is incorporated with fiducials. Phantom

experiments in the CT scanner and preliminary feasibility experiments in the MRI showing a targeting accuracy of 3.3 ± 1.7 mm in CT and 1.3 mm ± 0.8 mm in MRI.

Intending to reduce the radiation exposure of conventional X-ray guided procedures, and despite MRI environment-based robot system development challenges, (Li et al., 2019)[65] study presents the development of a 4-DOF lightweight with parallel mechanism body-mounted robotic system for MRI-guided low back pain injection. The system consists of a surgical planning workstation, a robot control, an MRI scanner, and a control console. The system-level accuracy was assessed with a phantom study showed 1.70 ± 0.21 mm mean value of target error. The system does not provide fully physical guidance since it is designed to provide 4-DOF motion to position and orient the needle, needle insertion is manually operated by the clinician, so it's still user-dependent and relies on the experience of the operator. Also, the influences of patient and respiratory motion were not considered in this experiment.

(Mokry et al., 2019)[66] evaluated the puncture cube system which is another patient-mounted system for CT-guided needle navigation and compared it to the free-hand method. The system consists of a patient-mounted self-adhesive cube and software that allows for needle guidance through the cube. The puncture cube (PC) has upper and lower templates, with several holes that offer stability for needle guidance as the needle is in contact to the corners of the holes but one of its limitations that only a discrete number of combinations for the needle trajectory are possible, there is a limit in combination and thus not every point below the PC can be reached.

In the planning phase, the PC is placed over the ROI, then the CT scan is performed and transferred to the system software which detects the location of the PC and superimposes the virtual cube model over the scanned PC. After selecting the target, the software calculates and displays corresponding holes through which the virtual needle passes for any given path in real-time.
To assess the accuracy and compare it with the freehand method, a phantom experiment was performed with 72 punctures. Results showed that the PCS punctures were more precise (mean error: 3.4mm vs. FHM 4.9mm) and it required less time and fewer control scans.

A summary of these studies is provided in table 2.8,2.9,2.10

Table 2.9: Summary of patient mounted robotic navigation systems

Study	Procedure	Image Modalities	Target	Experiment
Hata	Cryotherapy	MRI/CT	Kidney	Phantom study with motion simulation
Hungr		MRI/CT	Abdomen and thorax	Phantom study
Li	Injection	MRI	Low back	Phantom study
Mokry	Punctures	CT		Phantom with 72 punctures

Table 2.10: Summary of patient mounted robotic navigation systems accuracy - a

Study / System	Error Factors	Accuracy	
Hata	Probe placement error	No organ motion	2.1 ± 1.3 mm
		Organ motion	6.0 ± 3.1 mm
Hunger / Light puncture robot	Target error: the distance measured between the segmented needle tip and the planned target position	CT	MRI
		3.3 mm ± 1.7	1.3 mm ± 0.8 mm

	Angle error: the angular distance between the segmented needle axis and the planned needle direction	0.8 ± 0.7°	1.2 ± 0.6◦
Li	Target error: minimum distance from the desired target to the actual needle trajectory.		1.70 ± 0.21 mm
	Entry point error: the minimum distance from the desired entry point to the actual needle trajectory.		1.53 ± 0.19 mm
	Insertion angle error: a measure of an angular error between the planned and the actual needle insertion angle.		0.66° ± 0.43°

Table 2.11: Summary of patient mounted robotic navigation systems accuracy - b

Study / System	**Error Factors**	**Accuracy**
Mokry	The distance of the point of intersection of the needle with the plane lying coplanar to the surface at the depth of the target point to the target tip.	3.4 mm ± 2.3 mm

Table 2.12: Summary of patient mounted robotic navigation systems time

Study / System	Time	
Hata	No organ motion	11.9 ± 1.9 min
	Organ motion	14.0 ± 2.8 min
Mokry		168 s ± 28.5 s

Table, gantry, or floor-mounted systems, are another active systems type, these systems devices are designed to be fixed to the table, gantry, or floor rather than the patient. They provide physical needle guidance with the assumption that the patient's anatomy remains static throughout the planning and execution of the procedure not considering patient movement, respiratory induced organ motion.

Maxio is a robotic image-guided needle positioning system consisting of a treatment planning workstation and a robotic positioning device with a 5 DOF arm. (Abdullah, Yeong, & Goh, 2015)[67] study goal was to evaluate the technical success, safety, and performance level of liver thermal ablation using Maxio floor-mounted CT guided robotic positioning system on 20 patients with a liver tumor. During the procedure, patients were wrapped in reusable immobilizers to minimize their movement and respiratory motion control actions were taken. CT images then get transferred to the system workstation and the application software provides 2D and 3D visualization of data with lesion identification and segmentation process allowing for automatic volume calculation, and entry points defining along with a trajectory plan for the radiologist to check and confirm. The robotic arm gets activated and moved automatically to the desired location allowing the radiologist for ablation probe insertion. The 40 lesions experiment results show an average number of needle readjustment of 0.8±0.8 with no significant dose reduction between the robotic-assisted and the traditional method.

As discussed Maxio tasks were limited to needle placement and positioning with manual needle insertion. Unlike Maxio (Hiraki et al., 2018)[68] group at Okayama University has been working on Zerobot, an automatic needle insertion procedure, aiming to eliminate physician radiation exposure, by developing a controlled robotic system able to perform needle insertion under CT-guidance.

The system 6-DOF floor mounted robot consists of a manipulator includes an arm with an attached needle holder. The linear guide mechanism enables needle insertion and removal while a remote center of motion (RCM) functionality facilitates orientation. Great consideration of minimizing risks was taken by providing safety features represented in controllable emergency stop buttons, redundant encoders and force sensors, automatic risk control, and unintentional robot motion prevention features. Moreover, the RCM function is automatically activated once the button to initiate needle insertion is pressed in order to avoid tissue injury.

The robotic needle insertion procedure initiated by robot positioning and placement beside the CT table, then starting with needle targeting which can be performed both manually and then moving the robot needle tip to the determined entry point and angel, or in a semi-automatic mode where the robot moves automatically to position the tip of the needle once it's set by the physician. Hereafter the needle insertion phase begins with the ability to needle adjustment by the physician in case of target movement to ensure targeting accuracy. Besides, an ultrafast mode (approximately 500 mm/sec) is available for needle insertion.

The system accuracy was evaluated in both phantom and animals experiments. In the phantom experiment, the accuracy of the robotic needle insertion was equivalent to that of the manual insertion (mean accuracy 1.6 and 1.4 mm for robotic and manual insertion, respectively). And an overall mean accuracy of 3.2 mm in three swine experiments.

(Won, Kim, Kim, Seo, & Kim, 2017)[69] developed a CT table-mounted system for avoiding radiation exposure, a master-slave type robotic system for CT-guided needle intervention, that combines both tasks of a needle-path planning and a needle-inserting robot arm. It consists of a master console integrated with a user interface for monitoring the whole system, a slave robot with a 5-axis robot arm with an end effector, and a motor controller for needle insertion with real-time communication with the master console, and optical tracking systems. The system performed much better than laser-guided and freehand CT biopsy with an overall targeting error of 2mm which is also better than Maxio robotic system mean tip-to-target distance, which corresponds to the overall error of 6.5±2.5 mm.

A summary of these studies is provided in table 2.11,2.12

Table 2.13: Summary of table, gantry or floor-mounted robotic navigation systems

Study	Procedure	Imaging Modalities	Target	Experiment
Abdullah	Thermal Ablation	CT	Liver	20 patients, 40 lesions
Hiraki	Ablation, biopsy, and drainage.	CT-fluoroscopic	liver, kidneys, lungs, and hip muscle	Phantom and animal experiments
Won	Biopsy and RFA Ablations	CT & CT-fluoroscopic		abdominal phantom

Table 2.14: Summary of table, gantry or floor-mounted robotic navigation systems accuracy and time

Study / System	Error Factors	Accuracy	Time
Abdullah/ Maxio	The average number of needle readjustment	0.8 ± 0.8	nav: 01:16 min vs. control: 03:34 min
Hiraki / Zerobot		The accuracy of the robotic needle insertion in the phantom	

		experiment: 1.6mm In animals: overall mean accuracy of 3.2 mm.
Won	The minimum distance between the nodule center and the biopsy needle tip	2 mm

2.2.3 Biopsy Needle Navigation Systems

(Moche et al., 2016) [70] study aimed to evaluate the diagnostic accuracy of an optical tracking navigation device for MR-guided liver biopsies in a closed-bore scanner. The study was implemented on 52 patients who underwent MRI-guided needle biopsies of liver lesions using an add-on navigation system (iMRI Navigator) with optical tracking and automatic patient registration based on MRI-marker localization and a navigation display for needle movement tracking. Local anesthesia and breath-hold commands were performed to control organ motion. The procedure time was 51±12 min on average (range: 24–75 min) with a diagnostic accuracy of 92%.

(Treepong, Tanaiutchawoot, Wiratkapun, & Suthakorn, 2014) [71] work focus on path generation algorithm and interactive GUI to develop a navigation system for breast biopsy using Polaris®Vicra® optical tracking systems and a passive robotic needle holder to assist the operator with needle holding. 3D Slicer software was used for visualizing a real-time movement of 3D models and the GUI was developed on MATLAB.

The operator enters the position of the target and a real-time needle path visualization of the distance and orientation of the needle shows on the user interface for positioning guidance.

Their work proposes a path generation algorithm for needle insertion by considering the shortest way between the breast surface and cancer which is calculated for guiding the surgeon

to move the needle into the correct position and orientation. The proposed system is limited to a 3D phantom model lacking real organ potential error factors.

XACT robotic system is a real-time, CT-guided, three-dimensional system for minimally invasive, percutaneous interventional procedures. It was evaluated for precise percutaneous needle insertion by (Ben-David et al., 2018)[72]. an important feature of this device is enabling needle steering during stepwise correction of needle orientation based on the reconstructed CT images, the robot positioning unit can correct the trajectory by steering the needle during the procedure based on the deviation between the needle position and planned path.

It consists of an insertion module, robot positioning unit for steering the tool according to the trajectory. The system guides the tool according to a predefined trajectory. Guidance registration between the device and real-time CT images was performed using rigid-body registration, guided by CT-visible registration features on the robot.

Safety features were instituted, the robot automatically stops needle insertion when the required corrective angulation or motion of the needle potentially exceeds a predetermined threshold.

The evaluation experiment and simulated biopsies were performed on eight female Yorkshire swine, results showed a high targeting accuracy (< 3 mm), even for organs susceptible to deformation and respiration-induced motion.

ROBIO™ EX is another robotic positioning system that facilitates percutaneous needle placement during CT-guided interventional procedures, (Anzidei et al., 2015)[73] and has evaluated the performance of ROBIO for CT-guided lung biopsy.

A preliminary inspiratory breath-hold CT of the chest was performed using a breath-hold respiratory belt, the images were transferred to ROBIO™ EX workstation for biopsy planning, the target lesion and the entry point was determined by the operator, while the angulations of the needle, the depth of the target and the needle trajectory automatically calculated by the workstation and displayed in real-time. Once the plan is confirmed by the operator the robotic arm with a needle holder gets activated for needle insertion.

The study compared the performance of a lung biopsy CT-guided robotic system and the manual technique, results show that the use of robotic assistance reduced the procedural time and patient radiation exposure, but no major differences were found in the needle positioning precision, biopsy diagnostic performance complications rate.

(Lim et al., 2019)[74] URobotics Laboratory at Johns Hopkins has developed a table-mounted MRI compatible robot for bone biopsies under MRI guidance in the scanner improving traditional workflow and speed of the process.

The system consists of three main components: the robot, the interface box, and the robot controller. The robot orients a needle guide and the needle is inserted manually through the guide. Markers on the robot were used for MRI images to robot registration.

The system was previously evaluated on a phantom study which was convinced to move to the cadaver study, 10 locations in leg bones were targeted with an average accuracy of 1.43 mm.
A summary of these studies is provided in tables 2.13,2.14,2.15

Table 2.15: Summary of biopsy navigation systems

Study	**Image Modalities**	**Target**	**Experiment**
Moche	MRI	Liver	52 patients
Treepong	-	Breast	Breast Phantom
Ben-David	CT	lung, liver, kidney, and retroperitoneum	Non-randomized, uncontrolled preclinical animal study with 8 swine (45 needle placements)
Anzidei et al.	CT	Lung	with 100 patients (50 navigated and 50 freehand needle

Robio			placements)
Lim	MRI	Lges	10 biopsies of the femur and tibia in a cadaver leg.

Table 2.16: Summary of biopsy navigation systems accuracy - a

Study / System	**Error Factors**	**Accuracy**
Moche / iMRI Navigator	Sensitivity, specificity and diagnostic accuracy	88%, 100% and 92%
Treepong	Euclidian distance error	2.85 MATLAB GUI alone 3.69 MATLAB GUI & 3D slicer
Ben-David / XACT	Targeting accuracy: the distance between the needle tip and the target center.	1.8 mm ± 1.4 mm

Table 2.17: Summary of biopsy navigation systems accuracy - b

Study / System	**Error Factors**	**Accuracy**
Anzidei / ROBIO™ EX	Deviations on the x and y axes (mm)	x-direction: nav: 2.3 ± 1.1 mm vs. control: 3.0 ± 1.3 mm y-direction: nav: 2.5 ± 1.5 mm vs. control: 2.1 ± 1.6 mm
Lim	Targeting error: the	1.43 ± 0.52

	distance between the target in MRI and the projected line based on the CT data.

Table 2.18: Summary of biopsy navigation systems time

Study / System	**Time**
Moche / iMRI Navigator	24 – 75 min
Treepong	Average time only GUI 47.4 s Average time GUI & 3D slicer 37.2s
Ben-David / XACT	30 – 45 min
Anzidei / ROBIO™ EX	nav 20.1 ± 11.3 min vs. control 31.4 ± 10.2 min
Lim	41.32 ± 3.53 min

2.2.4 Biopsy Sampling Error

(Hodel et al.,2018)[10] conducted an experiment to examine (CT)-guided biopsy sampling errors in chondrosarcomas, the results showed high biopsy sampling error (14.7%) occurred in a total of ten patients.

Another study of 124 patients with chronic hepatitis C virus (HCV) infection who underwent laparoscopy-guided left and right lobe liver biopsies, 33% of cases had discordant results by at least one histologic stage.[25]

A group of 60 patients with hepatocellular carcinoma (HCC) liver cancer enrolled in (Forner et al.,2008)[38] study to evaluate the accuracy of the diagnosis of 2 cm or smaller nodules detected during ultrasound (US) screening. The false-negative rate of the biopsy was 30%.

(Sherman et al., 2016)[75] study also evaluates the accuracy of liver biopsy in patients diagnosed with hepatocellular carcinoma (HCC). The procedure was performed on 244 patients, false-negative biopsies found in 19.3% of the patients.

2.2.5 Liver Respiratory Motion

(Hata et al., 2016)[76] proposed a body-mounted robotic system for MRI and CT image-guided cryotherapy of renal cancer. A phantom validation study under phantom and organ motion imitation was performed for the proposed system assessment and compared with the freehand insertion approach. The findings of the study show that robotic system accuracy results outstand the freehand insertion, however, this advantage didn't exist anymore when target motion was introduced. The accuracy between the robotic 6.0 ± 3.1 and free-hand 5.9 ± 3.2 approaches becomes comparable when organ motion is presented confirming that organ motion as a source of error in needle interventions.

(Yoganathan et al., 2017) [77] discussed respiration-induced target motion in radiotherapy treatment and highlighted the adverse impact of organ motion on all the processes of radiation therapy, and confirmed the need for a method to control and encompass for target motion.

(Joe Y. Chang et al., 2008) [78] stated that respiratory tumor motion during radiation delivery is one of the main reasons for local failure after radiotherapy and a major obstacle, the study affirms the significance of considering tumor motion during radiotherapy due to the geometrical uncertainty it causes during radiation treatment.

(Clifford et al., 2002)[79] study was more specific regarding liver motion assessment and noted that percutaneous procedures in the liver such as ablation and biopsy require a relatively high degree of accuracy.

Research studies concerned about measuring organ motion displacement during respiratory, (Rohlfing et al., 2001)[80], analyzed liver motion by serial registration of MRI images and reported a significant translation between inspiration and expiration ranged from 12 to 26 mm. in the anterior-posterior direction range between 1-12 mm and in the lateral direction was between 1 and 3 mm.

Korin [81] study evaluates upper abdominal organs motion due to respiratory on 15 volunteers using MRI, recorded an average motion of liver 13 mm for normal breathing, and 39 mm for deep breathing.

Xi et al.[82] assessed the 3D motion of the diaphragm and abdominal organs of 13 patients using 4D CT. They reported a 10.1 ± 3.9 mm movement in CC direction for the liver which correlated well with the diaphragmatic movement. 1.2 ± 1.0 mm and 1.3 ± 0.5 mm for AP and LR directions respectively.
4D CT scans were acquired for 18 patients using an external abdominal marker for analyzing abdominal organs motion by Hallman JL et al. [83] The center of mass motion for liver clinical target volumes was 9.7 ± 5 (range 3-18 mm) in the superior-inferior direction.

Table 2.19: The mean and range of liver motion in Superior-Inferior (SI) / Cranio-Caudal (CC) direction in millimeters.

Study	Normal Respiration	Deep Respiration	Modality
Rohlfing	19 (12-26) mm	-	MRI
Korin	13 mm	39 mm	MRI
Xi	10.1 ± 3.9 mm	-	4D CT
Hallman JL	9.7 ± 5 (3-18 mm)	-	4D CT

2.2.6 Discussion

An overview of research studies regarding medical image processing clinical application, percutaneous needle navigation systems, biopsy sampling error, and liver motion as a source of error has been outlined and presented.

The studies experiments show that the use of image-guided navigation systems and different image processing techniques is an added value to the clinical interventions, and an effective assistance tool for the operators which contributes to disease diagnosing and tumor identification, pre-procedure planning, visual feedback, physical needle placement and

insertion in addition to passive guidance during procedures, increasing targeting accuracy, procedure efficacy and minimizing radiation exposure, outperforming by that the traditional interventions approach.

A diversity of modalities and technologies adopted in the literature studies can be observed, CT, MRI, and ultrasound is widely used as image-guided modalities in navigation systems, in addition to multi-modality approaches such as CT/MRI and PET/CT for better visualization quality. Also, navigation systems' extent of involvement and functionality varies between simple passive tools providing guidance only, to fully robotic systems that take control of needle placement and insertion which can also be categorized to the body and table-mounted devices. Different tracking navigation systems such as optical and electromagnetic have also been reported as instrument tracking technologies used in these systems.

The technologies used still encounter some limitations, major constraints can be found in optical and electromagnetic navigation systems, since they require an unobstructed line of sight or an undistorted magnetic field. Patient mounted systems perform under the assumption that the skin and target move as a rigid body, but this assumption does not work in all cases. Table, gantry or floor mounted occupy more space, increase set up effort, and change the clinical workflow.

Several prototypes of needle guidance systems have been developed and proposed in the literature. Nevertheless, their applications as commercial systems in clinics are less reported. This is often due to poor clinical applicability of these technologies which include technical non-friendliness and increased procedural complexity, set-up effort, and insufficient accuracy rates. Another reason for the limited adoption of such systems, the assumption of static target ignoring target motion due to respiration which results in needle targeting errors, or implementing breathing management techniques that increase patient discomfort.

The need to incorporate a method that eliminates error factors of target motion on needle targeting accuracy is still essential and could optimize the added value of needle navigation systems in percutaneous interventions. Especially for liver biopsy interventions which are still susceptible to relatively high biopsy sampling error and a large displacement magnitude of the liver during breathing as the studies show.

To overcome the current navigation systems limitations regarding biopsy sampling accuracy, equipment's step up effort and cost, neglecting organ motion as a primary source of needle interventions error, we propose a biopsy sampling navigation system compensates for organ motion during respiratory without the need to control or manage patient breathing, by utilizing computer vision techniques for tracking target movement during the procedure and controlling needle insertion based on displacement magnitudes. The navigation system motion-based controlled insertion is also integrated with procedure planning and accuracy evaluation modules built with imaging processing techniques to achieve an integral process with accurate results.

Chapter 3: Methodology

3.1 Study Design

The study used a simulation experimental study design following the biopsy sampling clinical procedure. The system was designed and implemented as a clinical flow procedure that allows physicians to create a patient-specific sampling plan before the sampling, and then the system automatically tracks and guides the needle during the sampling procedure.

The study patient data consists of ultrasound and CT images, nine ultrasound images were obtained from the ETHZ dataset, acquired at the Geneva University Hospital [84][85]. It comprises a scan of the liver of 9 volunteers acquired during free breathing over 5-10 min. The CT data were obtained from 3Dircadb (Research Institute against Digestive Cancer) database [86], composed of the 3D CT-scans of a female with 7 tumors.

CT images were used for testing the navigation system, motion detection, and tracking algorithms. The patient-specific treatment planning was created using the patients' CT images, while the motion was detected using the ultrasound dataset.

3.2 Software Development Environment

The navigation system was developed using the Medical Imaging Interaction Toolkit (MITK) as a fast prototyping open-source framework. The MITK is a free open-source software system providing extendibility by plug-ins development that interacts with the application core. It has been initially developed at the Division of Medical and Biological Informatics (MBI) at the German Cancer Research Center and was released in 2005 [87] as free open-source software under a BSD-style license.

The main focus of MITK is to enable the creation of highly interactive medical imaging software applications, it integrates different tools for medical imaging, computational modeling, computer graphics, deep learning, and numerical modeling for building applications with complex interaction mechanisms. It also provides a graphical user interface, multiple consistent views for the same data, 3D rendering, data retrieval, hierarchical organization for data objects, advanced visualization of multi-modal imaging, and support for 3D+t data.

MITK is an object-oriented cross-platform library implemented in C++ that supports Windows, Linux, and macOS. It integrates and extends widely-used open-source C++ libraries which are the Visualization Toolkit (VTK), and the Insight Toolkit (ITK) both supported by Kitware Inc.

ITK is an open-source, cross-platform library that provides an extensive suite of software algorithms for image analysis, it builds a set of fundamental algorithms especially for segmentation and registration. While the Visualization Toolkit (VTK) supports a wide variety of visualization algorithms and advanced modeling techniques.

In addition to ITK and VTK, third party packages can be integrated and used with MITK, such as the DICOM Toolkit (DCMTK, supported by Offis in Germany), and other commonly used C++ libraries (Boost, Qt, OpenCV among others). The software is designed to be extended via the addition of plug-ins, which are software entities that can be created using the C++ and connected to MITK general architecture.

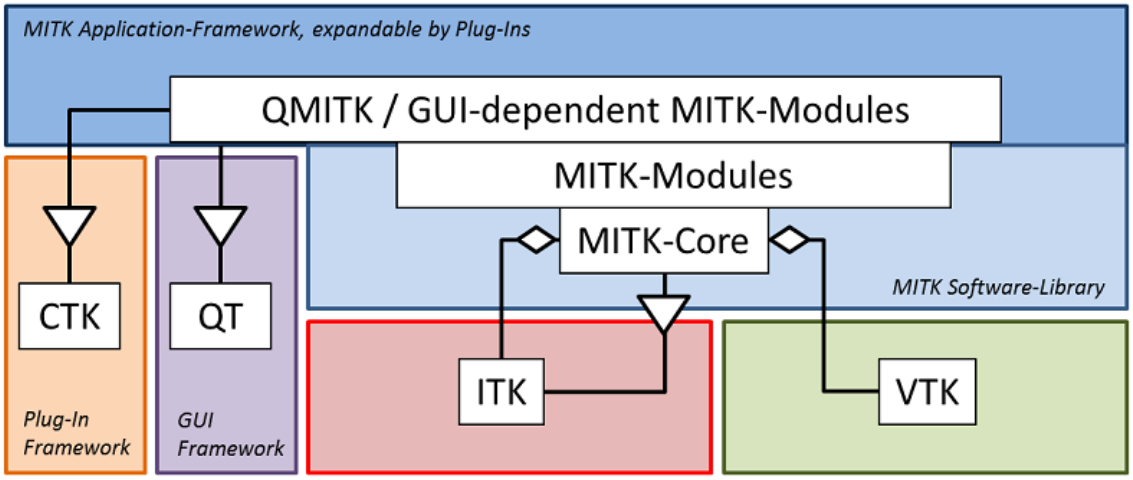

Figure 3.1: MITK Architecture and Main Libraries[88]

The architecture diagram in Figure 3.1, shows how MITK software library is strongly based on ITK and VTK functionalities. The addition of the QT GUI framework and CTK (Common Toolkit) plugin framework generates the MITK application where we can expand and add plugins.

In our software development, the MITK stable version (2018.4.99) that includes ITK, VTK, OpenCV, Boost, DCMTK, and Qt was used. The ITK and VTK were used in the development of patient-specific planning. The image segmentation and registration algorithms were used from the MITK development library, while we developed our algorithms for automatic needle path setting, needle motion control, and sampling error estimation. The MOSSE algorithm that is built-in OpenCV library has been used for motion organ motion detection.

3.3 Biopsy Sampling Navigation Plug-ins

Our navigation system used the advantages of CT/US image segmentation and registration algorithms. The CT image provides the physicians with detailed structural information of the ROI. While the US image used for respiration motion tracking and needle control procedure.

3.3.1 Biopsy Intervention Planning

The standard biopsy sampling clinical procedure was used for developing our patient-specific biopsy sample planning. The procedure starts from the ROI identification ended by tissue samples extraction. Figure 3.2 Illustrates the biopsy sampling of clinical procedure flow.

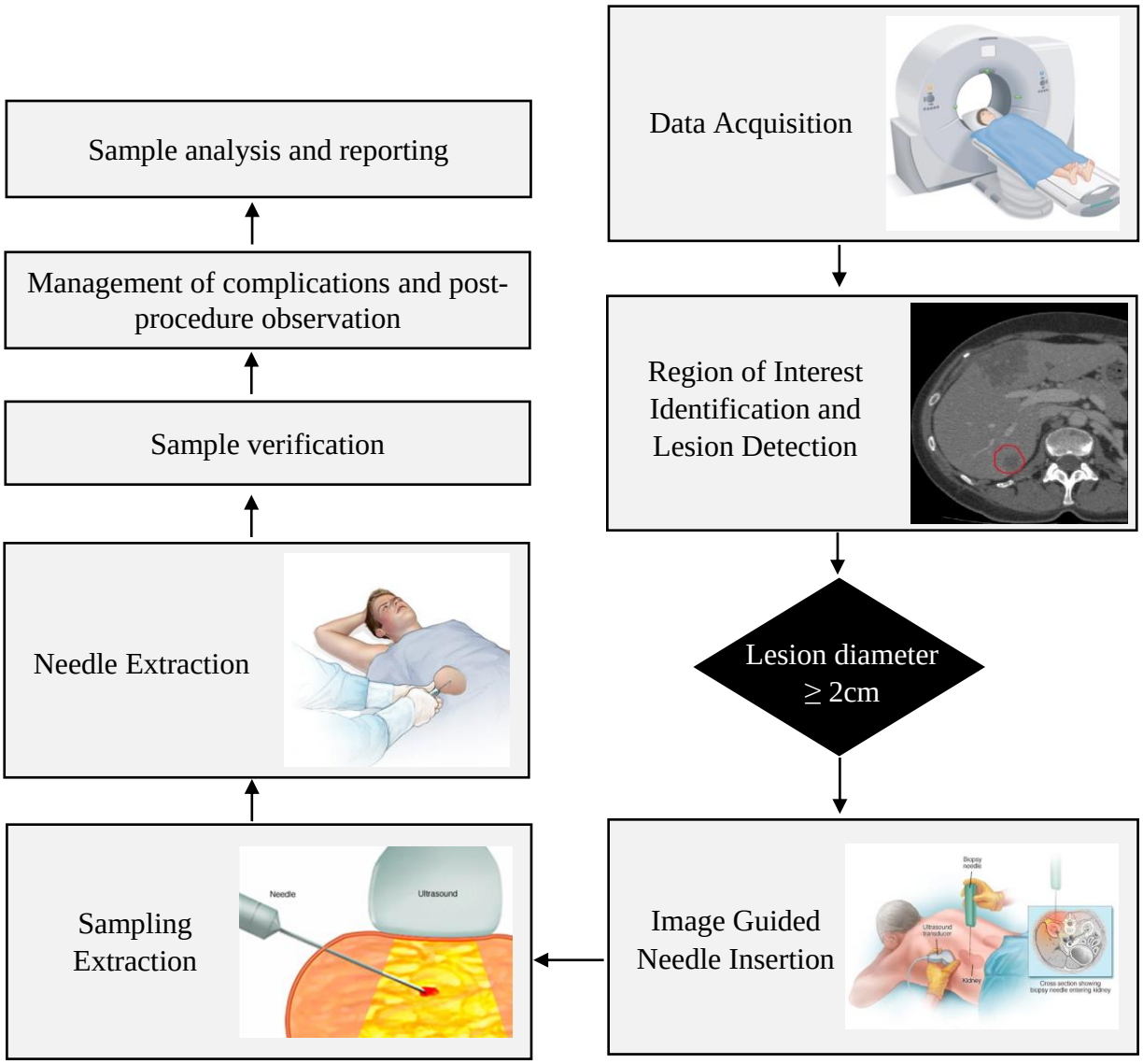

Figure 3.2: Biopsy Sampling Clinical Procedure Flow

The biopsy sampling clinical procedure starts with patient data acquisition using CT image modality scanning, then the lesion is identified and detected on the CT data if the lesion radius is ≥ 2 cm (based on our testing assumption for the experiments) it moves to the biopsy procedure.

Using image guidance, the operator starts the needle insertion process to reach the detected lesion and extract a tissue sample, once the sampling extraction is done, the operator extracts the needle out of the patient's skin.

The process then is followed by post-procedural actions, this includes complications management such as bleeding, pneumothorax, and visceral perforation, in addition to patient observation and monitoring his vital signs. After completing the procedure, the sampling tissue gets examined, and medically reported.

3.3.2 Region of Interest Identification

The MITK segmentation plug-in was used for providing physicians with the required segmentation tools to identify and segment the target region of interest. The interactive segmentation tool was used for this purpose. The tool has the image editing tool, the region growing, and the thresholding segmentation algorithms. It is a semi-automatic algorithm that combines manual and automatic segmentations:

a) The editing tool allows the user to add, delete, and modify the segmented ROI, while the region growing algorithm highlights the target region starting from a manual seeding point set by the user. Furthermore, the interactive tool includes the paint, wipe, and live Wire tools that enhance segmentation editing by painting or drawing the segment or wipe the painted voxels to exclude segments.

b) The semi-automatic Region Growing is a simple region-based image segmentation method. The algorithm approach relies on the assumption that adjacent pixels have similar color values or gray levels. It starts with an initial seeding pixel and then checking the neighboring pixels to determines whether to grow the region by adding the pixel neighbors to the target region if they have a similar gray value. It keeps iterating this process to scan the image pixels.[89]

   The algorithm procedure is as follows:

   Step1: Start with selecting a seeding pixel p_i

   Step2: Compute the difference of pixel value p_i and its neighboring pixel q.

   Step3: If the difference $|q - pi| \leq threshold$ merge pixel q to region segment R.

Step4: Repeat Step 2 & 3 for each of the newly added pixels. Stop if no more pixels can be added.

Simple Region Growing Algorithm

Initialize: p_i = seeding point, N = neighbors pixels set
R = region segment, T = threshold
Repeat
for each neighbor pixel q ∈ N
if $|q - pi| \leq T$ then
Add q to R
until N is empty

Figure 3.3: Simple Region Growing Algorithm Pseudocode

c) The thresholding algorithm is a widely used technique in image segmentation applications and a common segmentation algorithm that directly divides the image grayscale information processing based on the gray value of different targets.[90] The basic idea is to find an optimal gray-level threshold value based on image gray-scale distribution to separate objects of interest in an image from the background.

Assuming T stands for the global threshold of an image, thresholding is to get a binary image by turning pixels below T to zero and pixels above T to one, if f (x, y) indicates an image, g (x, y) is a binary image after thresholding.[91]

$$g(x,y) = \begin{cases} 1, & f(x,y) \geq T \\ 0, & f(x,y) < T \end{cases} \quad (1)$$

Thresholding operation is defined as:

$$T = M[x, y, p(x,y), f(x,y)] \quad (2)$$

Where T is the threshold, f (x, y) is the gray value of the point (x, y), p (x, y) denotes some local property of the point such as the average gray value of the neighborhood centered on the point (x, y).

On top of the MITK segmentation plugin, we have developed a segmentation statistical view that provides information about the selected segment to insight the operator about some important information. Once the segment is created, the user can select the desired segment and move to the statistics tab of our developed plugin and preview a summarized informative data about the selected segment. The segment statistics tab consists of three main tables, the first one shows the calculated segment area and volume in millimeters.

The second table provides the user with the 3D center point of the segmentation object. These centered coordinates automatically get saved and set as the target seeding point which can be optionally used or changed to another point value during the planning phase. The third table demonstrates the 3D segment object minimum, maximum, and range bounds on the x, y, and z coordinates. Segmentation statistics module is shown in Figure 3.4

The presented information is vital for the operator to evaluate the tumor dimensions, size, and position and takes an active guidance part for identifying the seeding point position in the planning step.

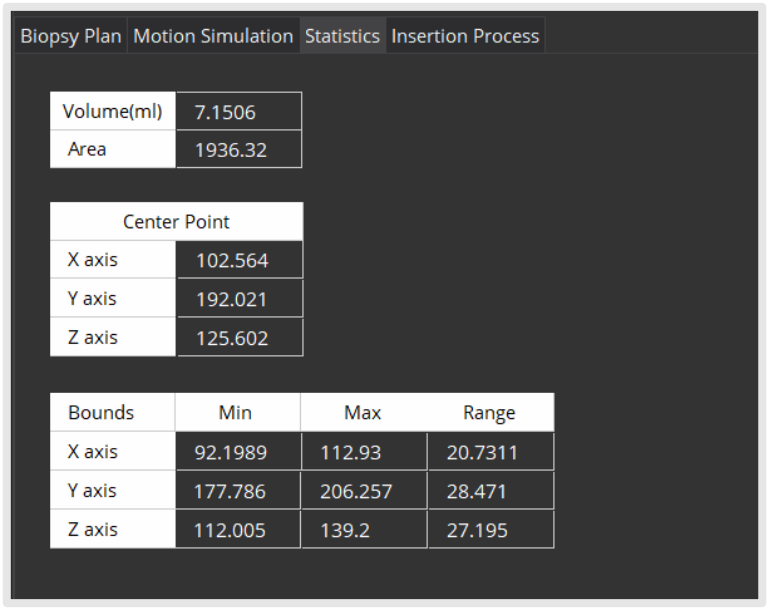

Figure 3.4: Segmentation Statistics Module

3.3.3 CT/US Image Registration

The MITK MatchPoint registration algorithm was used for achieving the image registration between the CT and US images. The image registration has been employed to benefit from the advantages of the two modalities. The CT image provides detailed structural information for needle navigation planning, while the US facilitates the real-time organ motion detection that is used for controlling needle navigation. The CT image is used as a reference image for patient-specific biopsy planning, where the real-time motion data will be extracted from the ultrasound image modality data.

The MatchPoint is a semi-automatic registration algorithm that is combined between the manual and automatic mapping and registration:

a) The manual registration tool allows users to configure the transformation settings of translation, scaling, and rotation over the three axes (sagittal, coronal, and axial) on the source image to adjust with the target image. The tool allows users to visualize matching and registration results with the ability to edit and adjust accordingly.

b) Affine registration algorithm was used for automatic registration. The affine transformations model is a linear transformation that consists of 9 parameters for managing scaling, rotation, shearing, and translation transformations [92]. Affine Transformation can be represented by a 3 × 3 matrix, Where R is the rotation matrix and t the translation vector.

$$T_{linear}(x) = R_x + t \quad (3)$$

The algorithm used the "Regular Step Gradient Descent" with "Mattes Mutual Information" for registration optimization. The mutual information is obtained by subtracting the entropy of both images from the joint entropy as:

$$\mathrm{I}(A, B) = \mathrm{H}(A, B) - H(A) - H(B) \quad (4)$$

Where H(A) is the entropy of image computed on the probability distribution of the grey values, H(B) is the entropy of image B, and H(A, B) is the joint entropy. Minimizing joint entropy leads to maximizing mutual information.

Mutual information can be used effectively on different image modalities registration cases and has been accepted as one of the most accurate and robust similarity measures for image registration.[93]

3.3.4 Needle Geometric Tool

A tool for biopsy sampling needle simulation was developed utilizing VTK geometry toolkit, the needle itself was simulated as a cylinder object with a radius and length entered by the user. The needle path was simulated by a cylindrical shape around the biopsy needle. The user can change the color and the opacity of both cylinders for differentiating between the two cylinders and to enhance the needle visualization.

The tool is developed as a semi-automatic needle simulation tool, where users can set the entry point by mouse click on the CT image, then the tool will automatically create the needle path starting from the entry point to the center of the lesion of interest. Figure 3.7 illustrates the needle insertion process on the patient CT image with a liver tumor.

The tool allows users to manipulate the needle path to avoid the critical structures and organs at risks such as bones, veins, and arteries, which can be done by scrolling through the image slices and making sure the trajectory path does not cross any critical structures. The tool allows users to set the needle parameters such as height, radius, and insertion angle, then the tool automatically generates the needle plan.

The following steps explain the needle insertion algorithm:

1) Path and needle radius: Which are the path cylinder radius and the biopsy needle radius that can be set by the user.
2) Path height: It is automatically calculated using the Euclidean distance between the insertion point and the center of the lesion of interest, figure 3.5 illustrated the height estimation.

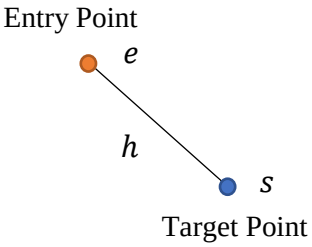

Figure 3.5: Needle Path Height Calculation

$$Path\ Height\ (h) = d(X,Y,Z) = \sqrt{(X1 - X2)^2 + (Y1 - Y2)^2 + (Z1 - Z2)^2} \quad (5)$$

3) Path angle, which is the insertion angle between the entry point and the center of the lesion of interest as illustrated in figure 3.6. The algorithm provides an automatic angle calculation for the needle by calculating the value of the inverse cosine of the dot product of the normalized vectors between the target point and insertion point.

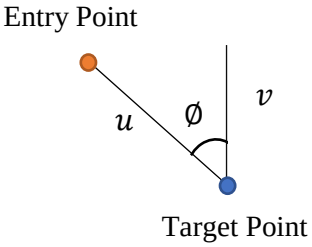

Figure 3.6: Needle Path Angle Calculation

$$\cos \emptyset = \frac{u \bullet v}{|u|\,|v|} \quad (6)$$

The tool provides four scenes viewer (axial, sagittal, coronal, and 3D), where the user can visualize the needle path planning from different views and angles. Figure 3.7 illustrates a real example of needle path planning using the CT image.

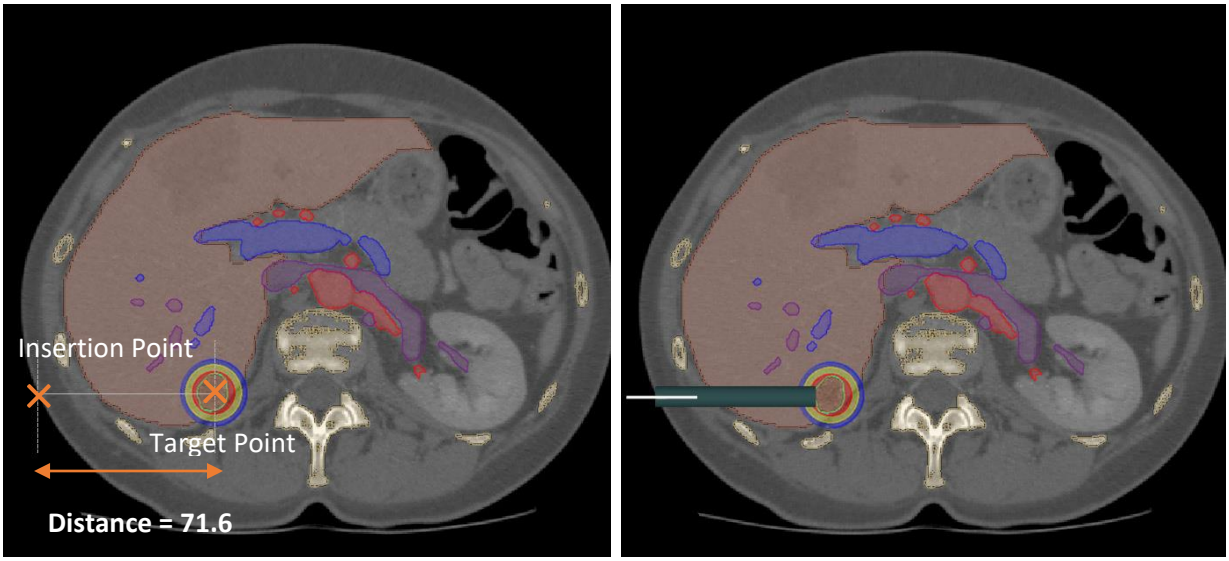

Figure 3.7: Procedure planning and path generation using the geometric tool

3.3.5 Biopsy Sampling Error Estimation

The biopsy sampling clinical procedure has identified several sampling types of errors that affect the sampling accuracy and increased sampling risks. Figure 3.8 illustrates the three major types of errors that might occur during biopsy sampling: The needle shift error, and depth error, and overall error.

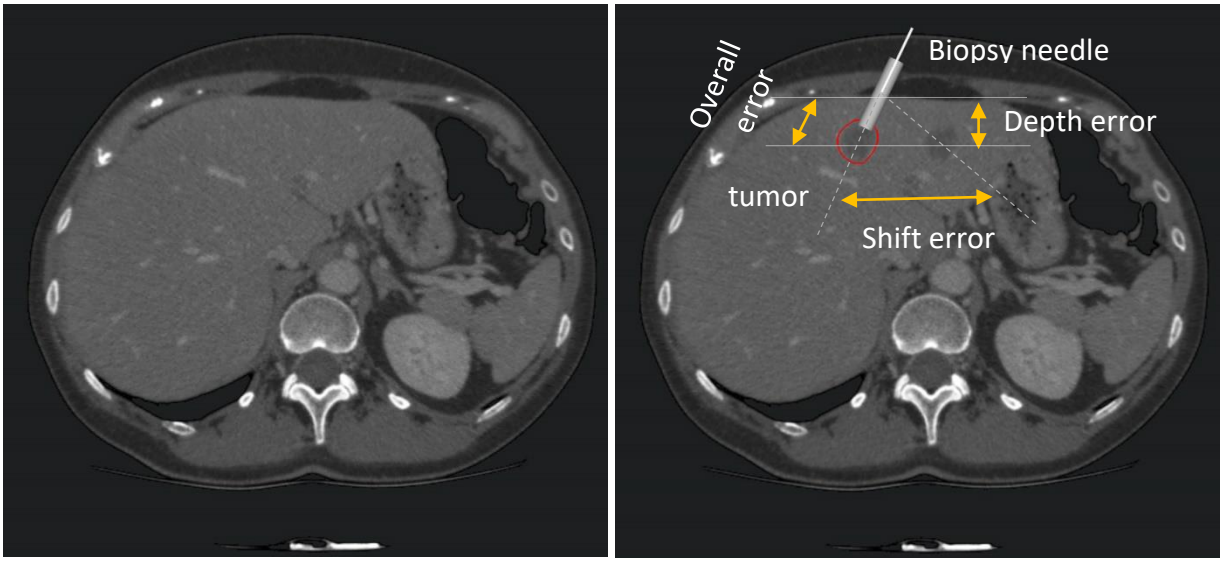

Figure 3.8: Illustration of the overall targeting error, the shift error, and the depth error

- The depth error is the vertical distance between the current needle tip (t) and the current target center (m).

$$Depth\ Error = t2 - m2 \tag{7}$$

- The shift error is the distance between the current position of the target center and the center position of the planned target region.

$$Shift\ Error = d(s,m) = \sqrt{(m1 - s1)^2 + (m2 - s2)^2} \tag{8}$$

- The overall error is the deviation in the Euclidean distance between the needle tip position and the current target center point.

$$Overall\ Error = d(t,m) = \sqrt{(m1 - t1)^2 + (m2 - t2)^2} \tag{9}$$

3.3.6 Organ Motion Tracking

The organ motion has been identified as one of the major sources of sampling errors in clinical application. In our system, the motion tracking was used as an innovative solution for controlling needle intervention source of errors. The US images were used for detecting and tracking organ motion. The OpenCV motion detection and tracking algorithms have been integrated into our navigation system. There are seven algorithms were used this purpose and implemented in the OpenCV library (Boosting, Multiple Instance learning, TDL, Medianflow, Kernelized Correlation Filter (KFC), Minimum Output Sum of Squared Error (MOSSE), and The Channel and Spatial Reliability Tracker (CSRT)). However, none of these algorithms were employed and used for tracking motion in US images for biopsy clinical application, therefore, we conducted a comparison study for comparing the effectiveness of these algorithms and selecting the best fit for our objectives.

1. **Boosting Tracker:** Boosting tracker a tracking method based on an on-line version of the AdaBoost algorithm which allows updating the group of features for the target object during tracking. Boosting classifier training is performed by updating the model with the positive and negative examples of the current frame, it marks the initial target area as a positive example and the negative examples are defined by taking regions from the background. [94]

   This method experimental results show a performance of (about 20 fps using a standard 1.6 GHz PC with 512 MB RAM)[94]

   The Boosting algorithm is a decade old and has been replaced by upgraded algorithms. There are no strength points attracted to use it, the tracker performance is slow and not reliable, that's why it was eliminated as a choice for our system tracking algorithm implementation.

2. **Multiple Instance Learning (MIL):** MIL is another approach for object detection, which is actually based on the boosting framework and also related to the work on online AdaBoost. However, it extends by presenting the basic idea of this learning paradigm where during training, examples are presented in sets called bags, and these bags get labeled instead of individual instances. When the bag contains at least one positive instance it's labeled as positive, if not the bag labeled as negative.[95] MIL tracker performance is good and more stable, it holds important information that avoids the mislabeling problem. Its approach outperforms boosting tracker by extracting a bag of potentially positive image patches and has the flexibility to pick out the best one.

3. **Kernelized Correlation Filters (KFC) Tracker:** Proposed by Henriques et al.[96], KFC tracker takes advantage of the large overlapping regions formed from multiple positive samples used in the MIL tracker. Faster and accurate tracking is achieved by exploiting the overlapping data and by extracting the Histogram of Gradient (HOG) features instead of raw pixels.

4. **TLD Tracker:** This method composed of three main components; the tracker component tracks the object in the frames. The detector localizes the observed appearances and

corrects the tracker as needed. Estimating the detector's errors is the learner's task to update and avoid these errors later. This method showed a better performance of precision in Kalal et al.[97] evaluation experiment over MIL tracker with a mean of 0.82 and 0.44 for TLD and MIL respectively.

5. **Medianflow Tracker:** Forward and backward in time tracking is performed by Medianflow tracker, and chooses the minimum forward-backward error trajectory for the succeeding tracking. [98] MedianFlow tracker is more suitable to types of problems when the object is visible throughout the whole sequence and object movement is consistent and predictable which is not the case organ motion in the ultrasound image.

6. **Minimum Output Sum of Squared Error (MOSSE):** MOSSE is a correlation filter tracker proposed by Bolme et al. [99], MOSSE tracker is more reliable and adaptable to different situations of lighting, scale, pose, and deformations compared to traditional approaches. In this tracker, the appearance of the target is modeled by adaptive correlation filters, and the tracking is implemented through convolution. The appearance of objects in filter-based trackers is modeled using filters trained on example images when the object gets selected in the first frame, the tracking, and filter training work together. MOSSE tracker overcomes the assumption that the target was always centered, thus providing a more flexible method. It shows to be an effective, simple to implement and a much faster tracking, that can operate at 669 frames per second.[99]

   As a correlation filter-based tracker, MOSSE track the target by correlating the filter over a search window in the next frame, using the fast Fourier transform (FFT) to calculate the correlation value. First, computing the 2D Fourier transform of the training input image $F = F(f)$ and filter $H = F(h)$. The convolution theorem states that correlation is the element multiplication in the Fourier domain. The correlation form is as follows where $\odot$ symbol represents element-wise multiplication, and * symbol indicates complex conjugate:

$$G = F \odot H^* \tag{10}$$

So, finding the filter template for tracking: $H^* = \frac{G}{F}$ (11)

MOSSE finds a filter H that minimizes the sum of squared error between the actual output of the convolution and the desired output of the convolution to find out the most possible location of the tracking object. The minimization problem formula is as follows:

$$min_{H^*} = \sum_i |F_i \odot H^* - G_i|^2 \quad (12)$$

Where F_i and G_i are the input images and the corresponding desired outputs in the Fourier domain and H is the filter that minimizes the sum of squared output error.[99]

MOSSE overcomes the occlusion problem, when the target is occluded, the algorithm determines the tracking object status and update the filter parameters based upon the peak-to-sidelobe ratio (PSR) value, so when the object is visible again it can be tracked again.

Figure 3.9 explained the MOSSE tracker on the liver ultrasound image. The algorithms tracked the liver motion caused by the patient breathing flow. Figure 3.9 (a). illustrates the identification of tracking region of interest. Figure 3.9(b) demonstrates that the algorithm missed the identified region due to the displacement caused by breathing. Figure 3.9 (c) illustrates how the MOSSE algorithm detects the region of interest due to organ backward motion.

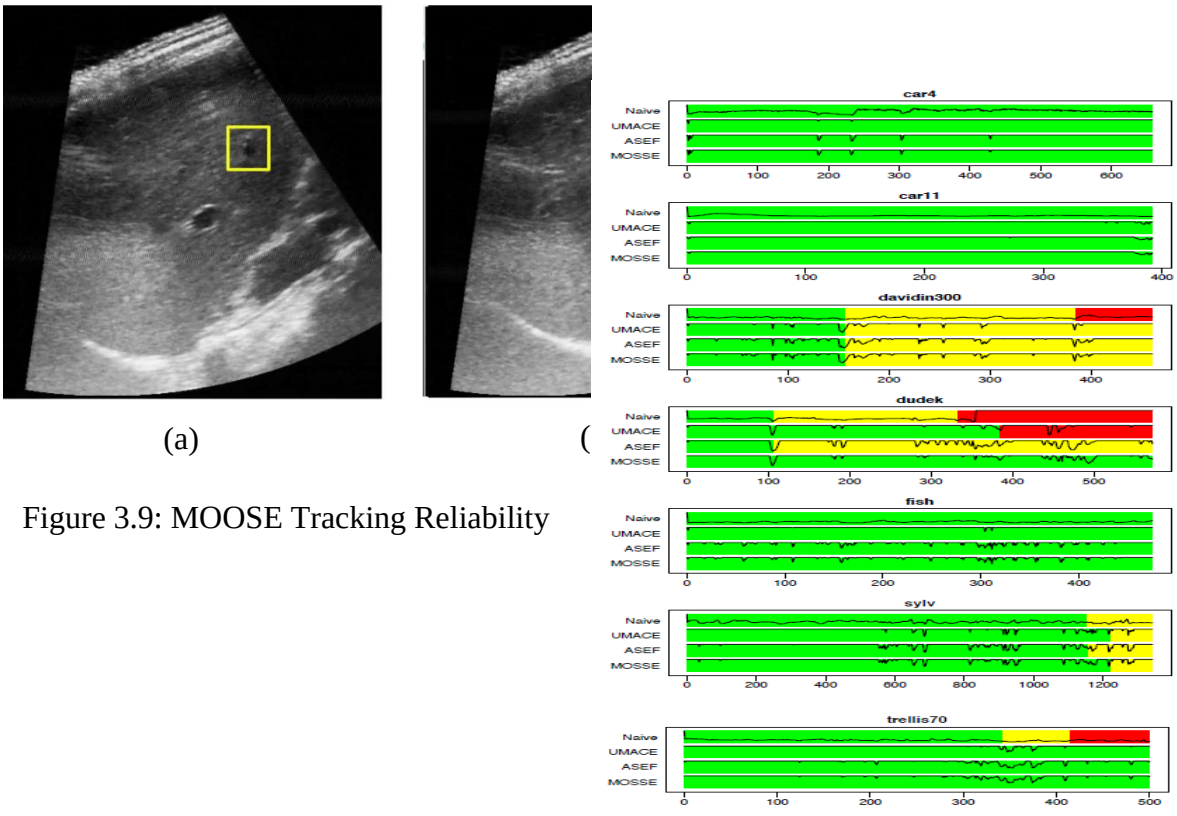

(a) (

Figure 3.9: MOOSE Tracking Reliability

Figure 3.10 shows the performance of the filter-based trackers including MOSSE on seven video sequences used for performance evaluation. Green indicates a good track, Yellow indicates the track drifted off-center, and Red indicates tracking failure. [99] Where it shows how MOSSE filter has outperformed the other three filters and didn't score any tracking failures in the seven tracking videos.

Figure 3.10: The performance of the filter-based trackers

MOOSE tracker was implemented in our system in C++ language and executed on a series of ultrasound DICOM sequences. The tracking cycle works as follow and demonstrated in Figure 3.11:

1. Once the ultrasound image first frame is received, the system converts it to an OpenCV image using MITK ImageToOpenCVImageFilter.
2. The previously planned target region area is marked automatically on the first OpenCV image and set as the region to be tracked.
3. By applying the MOSSE algorithm, the motion data, and the position of the tracked area on each frame is saved and reflected on the planned target volumes to move accordingly.
4. The image frame is rendered on MITK views, so the operator can view the ultrasound sequence and motion of target volumes on the system windows.

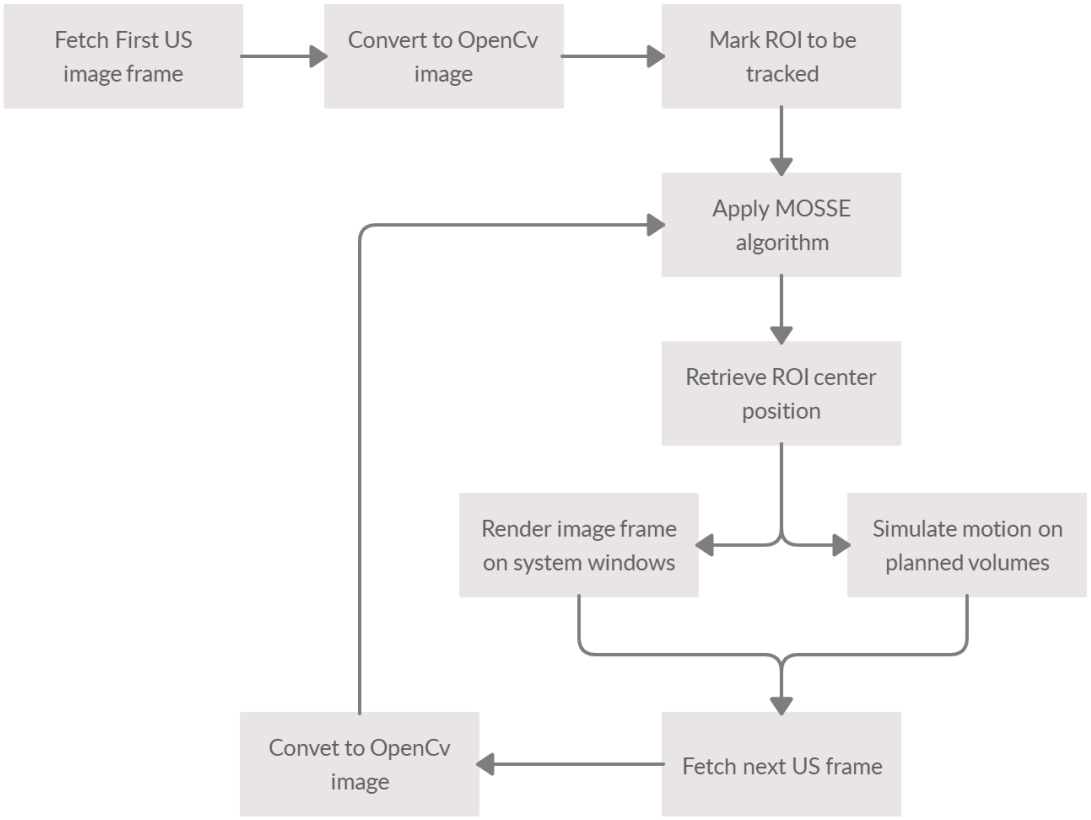

Figure 3.11: Flow Chart of Motion Tracking Implementation

7. **The Channel and Spatial Reliability Tracker (CSRT):** The Channel and Spatial Reliability Tracker (CSRT) is based on the Discriminative Correlation Filter (DCF) algorithm with introducing spatial and channel reliability (DCF-CSR) concepts.[100] Spatial reliability map usage is for tuning the filter support to the selected area from the frame for tracking, it also allows to expand the search region and enhance tracking of non-rectangular shaped objects.

To verify which tracking algorithm is more suitable for our navigation system, we examined these algorithms on real ultrasound data. The accuracy in object detection, the number of frames per second, and overall motion tracking time frame have been assessed and compared for the seven algorithms.

3.3.7 Patient-Specific Sampling Planning

A patient-specific treatment planning procedure has been integrated within our navigation system. The planning procedure was implemented based on a biopsy sampling clinical procedure. The procedure followed the radiotherapy treatment planning procedure in identifying the planning path. According to radiotherapy treatment planning, a three-volume of interest will be identified. The Gross Tumor Volume (GTV), The Clinical Tumor Volume (CTV), and the Planned Tumor Volume (PTV) [2] [101]. The GTV represents what can be seen from the CT image. The CTV is an additional margin for sub-clinical disease spread that can't be fully imaged and visualized by the human eye. The third volume is the PTV which is an additional margin for uncertainty in planning. Furthermore, the patient-specific planning procedure allows users to identify the target organ, organs at risk, and the trajectories around the needle path. Figure 3.12, 3.13 illustrate the patient specific sampling planning procedure.

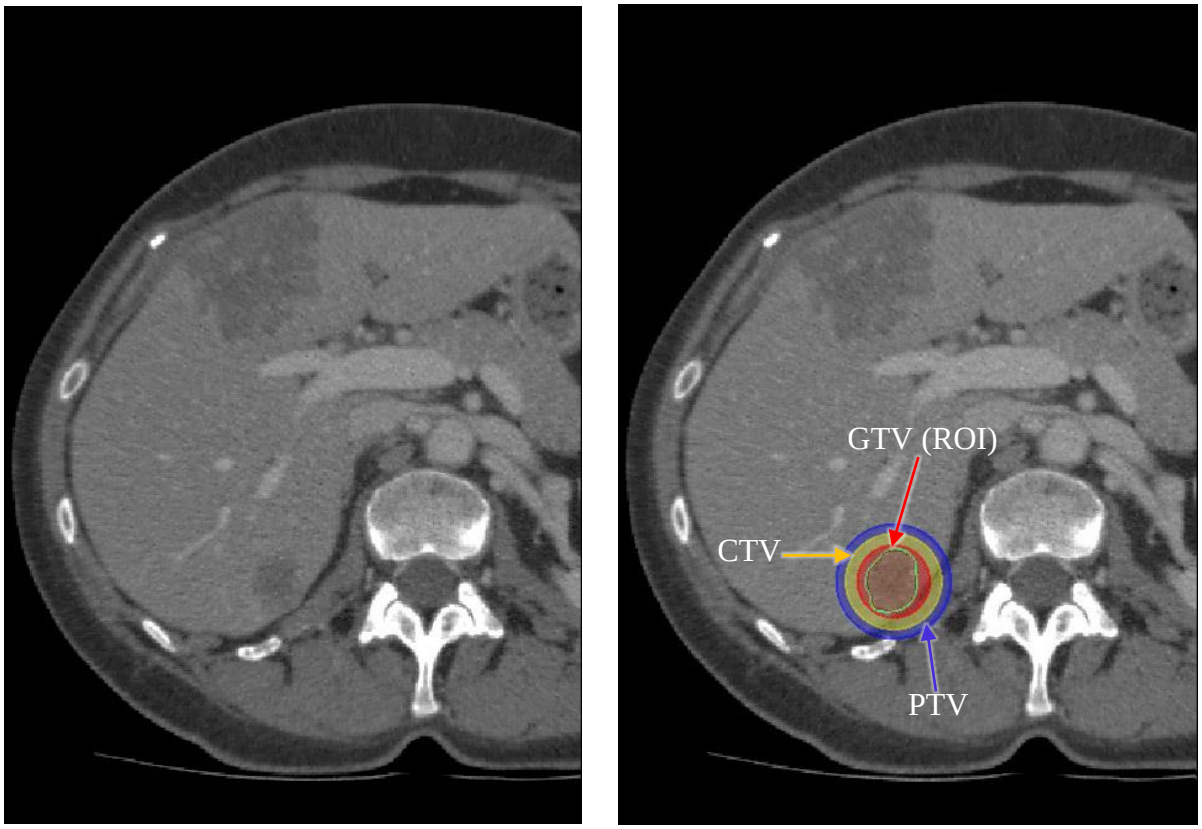

Figure 3.12: Biopsy Plan with GTV, CTV, PTV

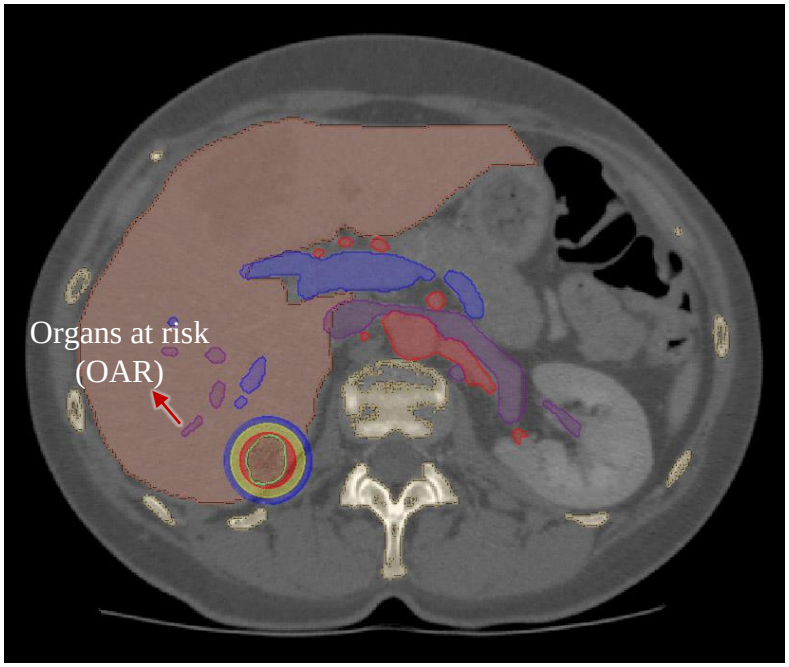

Figure 3.13: Biopsy Sampling plan avoiding organs at risk

The margin distance between the three volumes was set using the following:

1. The segmentation statistical tool data presented in Figure 3.4, which provides the needed geometric information for determining volume, area, dimensions, and bounds of the segmented volume.
2. The CTV-PTV margin was determined following organ motion peaks. The average motion peaks were considered in identifying the uncertainty levels. The distance between the three volumes considered the disease spread coverage and the motion threshold. The tool provides users with the average shift error in x and y direction about organ motion. The formula 10 explain the average distances in X -Y direction through the image slices.

$$\bar{x} = \frac{\sum_{i=1}^{n} x^i - x^0}{n} \qquad \bar{y} = \frac{\sum_{i=1}^{n} y^i - y^0}{n} \tag{13}$$

n: number of tracked ultrasound slices

3.3.7.1 Needle Insertion Control Algorithm

Needle Insertion workflow allows physicians to identify the needle trajectory according to the planning procedure. The needle insertion control algorithm starts when the physician clicks the start button on the control panel. The insertion process starts with action from the operator by clicking on the start insertion button on the system window. When the operation starts, the system calculates depth and shift error based on the ultrasound tracked motion data. Regarding these error calculations, the system decides to insert or pause inserting.

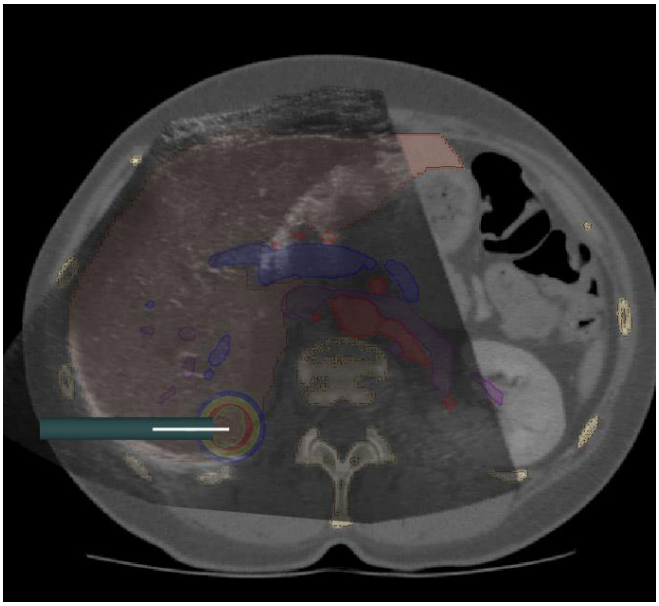

Figure 3.14: Needle insertion process

The procedure involves the incremental insertion of the needle along the planned trajectory, if the needle tip doesn't reach the target point yet (floor (depth error) = 0 OR needle Y position > target Y position) AND the shift error is less than the allowed margin T, then the needle insertion starts following the planned path. However, if one of the conditions fails, needle insertion is paused until the failed conditions are resolved.

$$insert(t,m) = \begin{cases} 1, & Shift\ error\ < T\ \ AND\ t2 \ncong m2 \\ 0, & Else \end{cases} \quad (14)$$

During the insertion process, the operator keeps tracking the target motion with ultrasound visualization. The system notifies the physician when the needle insertion process stopped. All error calculations, depth error, target error, and overall error with the current positions of needle tip and target center point are also displayed on the operator screen during the intervention. When the needle tip hits the target lesion, the insertion process is considered complete and ready for tissue extraction as illustrated in figure 3.14

Chapter 4: Experimental Results and Analysis

4.1 Motion Tracking Algorithms Comparison Results

A comparison study has been conducted for comparing the performance and the speed of the six motion tracking algorithms. The study includes ultrasound video data for four patients. The video data resolution was 712X480, 16 farms/second, and 2MHz center frequency with a period of one minute. The experiment was conducted on a laptop computer with 1.8 GHz CPU and 8 GB RAM running on Windows 10 operating system.

The ROI for tracking was identified by drawing a 5mm bounding box on each video. The six algorithms that were executed on the 4 videos as illustrated in table 4.1. The rate of processed frames per second was estimated for each algorithm. Results indicated that the MOSSE has the highest rate of processed frames/second. On average the MOSSE processed about 92 frames/second while the rest of the algorithms processed ≤ 16.5 frames/second.

Table 4.1: Speed comparison of six trackers on a video sequence in terms of FPS

Patient / Tracker	**MIL**	**KCF**	**TLD**	**MEDIANFLOW**	**MOSSE**	**CSRT**
Patient 1	1.31	11.76	0.28	16.66	100	2.98
Patient 2	1.32	14.28	0.92	18.18	100	3.12
Patient 3	1.29	18.18	0.92	14.28	66.66	2.81
Patient 4	1.35	14.28	0.52	16.66	100	3.03
Mean	**1.32**	**14.62**	**0.66**	**16.45**	**91.66**	**2.98**

For accuracy assessment, 10 lesions were defined and tracked on 10 different ultrasound video data, and the accuracy evaluation considered (good, bad, failure) as follows:

- Good: tracking bounding box covering the lesion correctly.
- Bad: the tracked lesion is not centered or accurately tracked in the bounding box.

- Failure: the tracker either reported failure and can't detect the lesion, or the intended lesion is totally out of the bounding box.

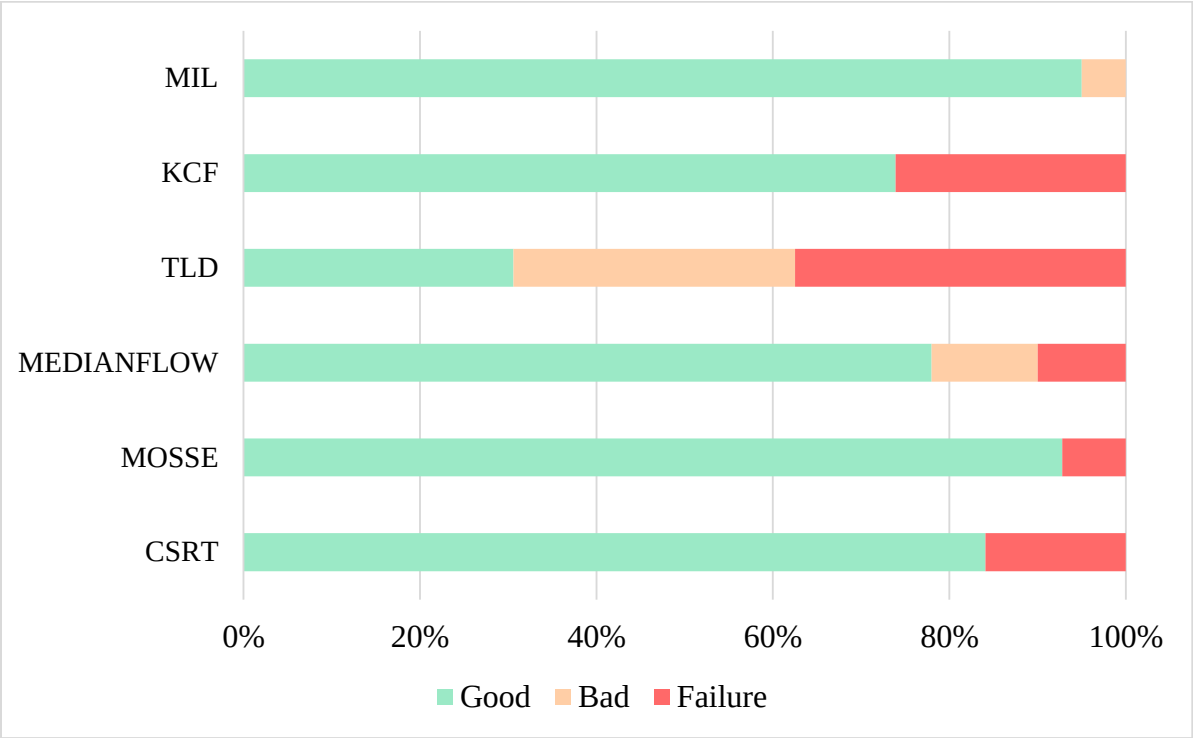

Figure 4.1: Tracking Accuracy Evaluation

Figure 4.2 shows the accuracy evaluation for the 6 tracking algorithms, the results show that MIL, MOSSE and CSRT achieved high good tracking accuracy rates of (95%, 92.8%,84%) respectively, unlike TLD with the lower good tracking rate (30.6%) and highest failure rate detected (37.5%)

Considering both tracking speed and tracking accuracy, MOSSE was the most suitable algorithm for real-time ultrasound image-based tracking problems, with the highest speed and good tracking accuracy.

4.2 Needle Tracking Simulation Results

The needle tracking system was examined by conducting a clinical workflow biopsy sampling experiment on a sample of 9 patients with liver ultrasound images. The sampling time, success rate, the overall error was estimated for evaluating the navigation system efficiency. Table 4.2

illustrates the lesions of interest area and location for the nine patients. Three lesion diameters were set ranging from 2cm to 6cm for the nine patients, producing a region of interest area ranged from 3.14 cm- 28.3cm^2. The locations of these lesions were superficial and deep-seated patient liver. The superficial was (3.5- 10.9 cm) away from the patient outer skin, while the deep-seated was 11.8-17.0 cm away from the patient outer skin. Furthermore, the distance from organs at risk was considered and identified. The minimum and maximum distance found was (20mm- 148mm) respectively.

The respiratory impact on the liver motion was measured for the nine patients. Table 4.2 shows the quantitative data on liver respiration motion. The data was measured using the motion detector MOSSE algorithm. The average minimum and maximum amplitude (mean ± standard deviation) for all patients was ranged from (7.2 ± 3.1) to (30.2 ± 20.73) respectively. The maximum average motion amplitude found was 41.8 mm. Furthermore, the respiration average speed was measured for the nine patients, the minimum and maximum speed found was 0.12(mm/s) to 0.37mm/s.

Table 4.2: Quantitative data of liver respiration motion during 1 minute of breathing

Patient Number	**Average Motion Amplitude (mm)**	**Average Motion Distance (Mean±SD) (mm)**	**Average Speed (mm/sec)**
1	10.3	7.2 ± 3.1	0.12
2	18.1	8.9 ± 5.8	0.15
3	31.5	19.3 ± 9.7	0.32
4	41.8	30.2 ± 20.7	0.5
5	16.8	10.2 ± 5.7	0.17
6	22.3	11.6 ± 7.8	0.19
7	29.6	22.2 ± 9.7	0.37
8	18.9	11.8 ± 5.4	0.19
9	12.9	9.4 ± 4.9	0.15

Tables 4.3-4.5 show the needle depth and the region of interest distance from organs at risk. For the 2,4 and 6 cm lesion of interests. The min and max depth found was ((35.5-196.6); (52.3-228); (109- 200.87) mm) respectively. While the min and max distance away from the organ at risk was ((7.4-22) ;(8.2-23) ;(11.9-28.2) mm) respectively.

Table 4.3: 2 cm lesions of interests with 3.14 cm^2 area location and path length for the nine patients

Patient Number	Depth (mm)	Distance from the nearest organ at risk (mm)
1	35.5	11.00
2	191.6	22.00
3	196.60	16.18
4	174	10.41
5	132.97	7.36
6	105.59	11.71
7	174.00	15.19
8	138.05	17.25
9	143.00	8.98

Table 4.4: 4 cm lesions of interests with 12.57 cm^2 area location and path length for the nine patients - a

Patient Number	Depth (mm)	Distance from the nearest organ at risk (mm)
1	52.3	23.00
2	228	10.19
3	122	16.6
4	162.5	16.8

Table 4.5: 4 cm lesions of interests with 12.57 cm^2 area location and path length for the nine patients - b

Patient Number	Depth (mm)	Distance from the nearest organ at risk (mm)
5	184.39	13.64
6	91.00	11.85
7	107.38	8.22
8	180.00	10.38
9	213.19	14.48

Table 4.6: 6 cm lesions of interests with 28.27 cm^2 area location and path length for the nine patients

Patient Number	Depth (mm)	Distance from the nearest organ at risk (mm)
1	166.09	28.17
2	200.87	12.8
3	180.28	12.69
4	198.25	22.18
5	147.00	11.9
6	120.34	13.74
7	175.17	19.18
8	154.2	15.55
9	109.77	23.42

Table 4.6 shows the experiment result for the nine patients. One mm needle diameter was used for tissue sampling. Three motion detection thresholds ranged from (1.5-4.5) were used

depending on respiratory motion speed. The sampling planning path was determined based on the lesion location and the best entry point. Patient-specific sampling plans were planned using the CT images before the sampling procedure application. The patient's plans were set for avoiding ribs, bones, organs at risk (veins or arteries).

Table 4.7: Experiment sampling error results for 2 cm lesions

Patient Number	Motion Threshold	Insertion angle	Shift Error	Depth Error	Overall Error	Mean Motion	Time (minutes)
1	1.5	22	1.00	1.19	1.29	2.6	4.2
2	2	45	1.41	0.55	1.56	9.77	15.5
3	3	45	1.41	1.28	1.81	13.2	20.6
4	5	45	2.82	0.43	0.58	18.8	14.5
5	4.5	90	4.12	1.00	1.41	12.10	22.48
6	2	35	2.00	1.17	1.65	14.96	9.6
7	2	90	2.00	0	2.00	13.03	12.79
8	1.5	70	1.41	0.97	1.83	8.38	18.8
9	2	14	1.41	0	1.00	11.21	15.01
Mean					**1.45**		

Table 4.8: Experiment sampling error results for 4 cm lesions - a

Patient Number	Motion Threshold	Insertion angle	Shift Error	Depth Error	Overall Error	Mean Motion	Time (minutes)
1	2.5	64	1.41	0.71	1.11	2.09	2.6
2	3	90	1.41	1.00	1.41	6.97	11.7
3	2.5	90	2.23	2.00	2.82	9.7	9.4
4	2	22	1.00	0.08	2.31	5.00	8.7

Table 4.9: Experiment sampling error results for 4 cm lesions - b

Patient Number	Motion Threshold	Insertion angle	Shift Error	Depth Error	Overall Error	Mean Motion	Time (minutes)
5	4	17	2.00	1.58	2.07	8.32	15.3
6	1.5	90	1.00	1.00	1.00	6.53	12.4
7	5	58	1.00	0.32	0.86	12.60	5.5
8	3	90	2.23	1.00	2.23	10.5	10.7
9	2	60	1.41	0.48	3.16	14.08	12.06
Mean					**1.88**		

Table 4.10: Experiment sampling error results for 6 cm lesions

Patient Number	Motion Threshold	Insertion angle	Shift Error	Depth Error	Overall Error	Mean Motion	Time (minutes)
1	1	17	1.00	0.69	1.25	4.32	8.2
2	3	32	1.00	0.07	0.89	7.6	9.6
3	2	18	1.41	1.21	1.26	12.35	13.6
4	3	10	2.23	0.78	2.38	7.86	8.68
5	4	90	3.16	1.99	3.56	6.91	7.8
6	2.5	43	2.00	0.44	1.58	9.78	10.1
7	3.5	50	1.00	0.65	1.55	14.39	9.8
8	3.5	40	2.24	0.18	3.63	6.82	11.14
9	3	17	1.00	0.8	1.83	11.8	12.5
Mean					**1.99**		

Table 4.6 shows the results of the biopsy sampling error for the 2cm lesion of interest. The results indicated that the overall average sampling error found was 1.5mm for the nine patients. The minimum and maximum overall biopsy error found was (0.6 to 2.0 mm) respectively. The minimum and maximum sampling time found was (4.0, 22.5) minutes. The overall average time was 14.8 minutes.

Table 4.7 shows the results of the biopsy sampling error for the 4cm lesion of interest. The results indicated that the overall average sampling error found was 1.9mm for the nine patients. The minimum and maximum overall biopsy error found was (1.0 to 3.2 mm) respectively. The minimum and maximum sampling time found was (2.6, 12.1) minutes. The overall average time was 9.8 minutes.

Table 4.8 shows the results of the biopsy sampling error for the 6cm lesion of interest. The results indicated that the overall average sampling error found was 2.0mm for the nine patients. The minimum and maximum overall biopsy error found was (0.9 to 3.6 mm) respectively. The minimum and maximum sampling time found was (8.0, 13.6) minutes. The overall average time was 10.2 minutes.

A showcase of an experiment is presented in Figure 3.16(a), where the target tumor and the organs at risk are segmented on the CT image, in addition to the biopsy plan set up with the needle trajectory connecting to the target lesion (in brown). In Figure 3.16(b) the ultrasound image is registered and fused with the CT image for target motion tracking and needle

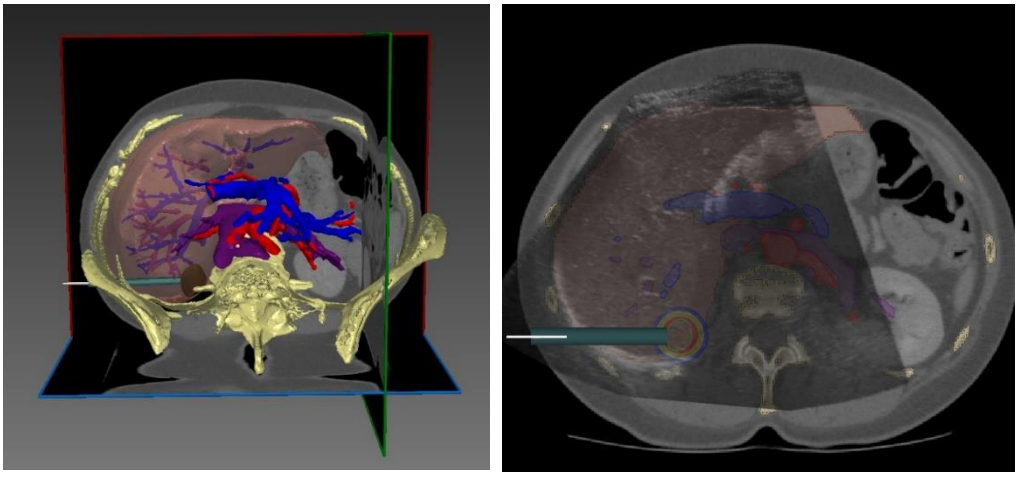

insertion.

(a) (b)

Figure 4.2: Showcase of segmentation and registration experiment

Chapter 5: Discussion and Conclusion

5.1 Discussion

Corresponding to our objectives, a liver biopsy needle navigation system was designed and developed ensuring clinical applicability and overcoming patient-specific procedures limitations and challenges by proposing methods for organ motion compensation utilizing computer vision, enhancing by that the overall procedure efficacy and accuracy, and minimizing biopsy sampling error thus post-procedural complications.

Multiple studies have been investigating solutions for percutaneous needle interventions and biopsy procedures, however, as discussed in Chapter 2 literature, major challenges and lack of clinical applicability of these solutions still present. One of the main distinguishing features of our proposed solution, is following the clinical requirements without the need to change the workflow or set up complex expensive equipment and devices, most of the previous studies require the use of either optical or electromagnetic devices for tracking and registration, in our system no additional devices is needed, maintaining no extra cost or further requirements, not only adapting to the current clinics workflow, but also providing methods for overcoming existing clinical limitations with image-guided organ motion tracking and respiratory induced motion compensation during the intervention, which is not accountable by most of the previous navigation systems proposals, or only treated by performing breath-holding techniques and respiratory management methods but not actually finding a way to adapt with during procedures, unlike our proposed novel method for controlled needle insertion based on target organ motion tracking from the ultrasound imaging modality using computer vision algorithms.

Utilizing OpenCV tracking MOSSE algorithm was a successful fulfillment for our objective and main contribution which is outlined as being able to track and get the position of the target region which is subjected to large shifting displacement during liver biopsy procedures and has not been examined or proposed in the previous studies. Computer vision and it's application in medical image processing for guided needle interventions showed to be an added value to clinical procedure and allows for internal organ movement tracking directly

form the ultrasound real-time image modality with a sufficient accuracy and high reliability regardless the image quality and light reflections situations with a high tracking speed.

Integrating our computer vision solution for organ motion tracking with a geometric tool for biopsy patient-specific planning including lesion of interest segmentation, CT-ultrasound image registration, path creating, needle orientation and adjustment, automatic controlled needle insertion by tracked target position and displacement, have produced an accurate full functional biopsy image-guided navigation system for pre-procedural planning, intra-procedural needle control and management, and post-procedural assessment and evaluation.

The developed system targeting accuracy was experimented and evaluated on 9 patients' data with a total of 27 experiments that vary between 2 cm,4 cm, and 6 cm lesions radius. To assess the accuracy, the overall targeting error used which defined as the deviation in the Euclidean distance between the needle tip position and the current target center point. The mean overall error found was 1.45,1.88,1.99 mm for the three different lesions radius respectively, and an overall mean targeting accuracy for the 27 experiments of 1.78 ± 0.8 mm which is a higher accuracy than XACT robotic navigation system (1.8 mm ± 1.4 mm) [72], Zerobot CT guided robotic system accuracy results on animals (3.2 mm) [68], Mokry's patient mounted system with (3.4 mm ± 2.3 mm) [66] and AxiEM for 1mm, 3mm, 5mm slice thickness (3.86 ± 2.28, 3.74 ± 2.1, 4.81 ± 2.07)[62] and IMACTIS (3.7 mm)[59] electromagnetic systems. The results also outperform the optical tracking-based navigation systems in Engstrand study (4.0 ± 2.5 mm)[56] and Oliveira-Santos's (3.1 ± 1.2 mm) [55]. The other systems that scored better results such as Li's [65] body-mounted robotic system and Lim's [74] body-mounted system were evaluated on static phantoms and cadavers with no motion introduced which justifies that accuracy achieved.

Our proposed system preliminary results are promising and showed relatively high accuracy with normal free-breathing and no control over the breathing patterns comparing to the accuracy results of the previous studies.

5.2 Conclusion

This thesis has presented a clinically applicable biopsy navigation system solution, providing the operator with the tools needed to achieve an accurate safe biopsy procedure with no control needed over the patient's breathing and achieved a high overall targeting accuracy.

The main focus of the research is to explore and examine methods to eliminate organ motion sources of error in liver biopsy procedures. A new approach based on computer vision image-based tracking was introduced to compensate for organ motion and associated control of needle insertion to solve the problem of mistargeting in percutaneous interventions.

The system design and integration with computer vision have accomplished a major contribution regarding controlling needle insertion by organ motion tracking during percutaneous interventions. Chapter 3 discussed the system's components and the tools provided to achieve the overall biopsy clinical process application.

The system has been validated by accuracy comparison with previous studies needle navigation systems proposals discussed in Chapter 2. 27 simulated liver tumor biopsy sampling experiments were conducted and reported with a mean overall error of 1.78 ± 0.8 mm which outperforms navigation system results on static targets.

The literature and the experiment confirm that organ motion is a major source of error during interventions and eliminating and control the motion factor with patient-friendly methods majorly contribute to improve the needle targeting accuracy and minimize the deviation between the planed and the final needle position, as well as sampling error in a reasonable intervention time.

Ultrasound imaging modality usage for organ motion tracking was sufficient enough to control needle insertion and archive the needed targeting accuracy for procedural success, integrated ultrasound CT imaging modalities also improved the planning process with minimal radiation exposure.

5.3 Future Work

Different tests and several experiments on real patient's data are intended to be conducted in the future, considering more cases and breathing patterns and exploring different patients' health situations, as well as automating threshold calculation based on patient-specific respiratory speed and patterns.

We seek to expand the scope of this system and integrate it with real-time ultrasound devices, to be able to implement real-time data grabbing, analysis, and processing to achieve a full-integrated clinical ultrasound image-guided system. We also looking forward to automating the system and integrate our software with robotic devices to eliminate freehand needle placement error and any human source of errors, considering personal control and operator intervention when needed.

Examining and exploring methods and algorithms for automatic accurate fast CT to ultrasound image registration is one of the next steps to take to improve the semi-automatic registration phase in our system and to be able to extract the most of the features from the different modalities combined. Not limited to that, we additionally consider developing an automatic optimal path planning tool using image processing techniques to avoid organs at risk and critical structure ensuring the most optimal possible trajectory for the procedure.

References

[1] Q. Zhang and H. Xiao, “Extracting Regions of Interest in Biomedical Images,” *Futur. Biomed. Inf. Eng. Int. Semin.*, vol. 0, pp. 3–6, Dec. 2008.

[2] N. G. Burnet, S. J. Thomas, K. E. Burton, and S. J. Jefferies, “Defining the tumour and target volumes for radiotherapy,” *Cancer Imaging*, vol. 4, no. 2, pp. 153–161, 2004.

[3] A.-L. Grosu, L. D. Sprague, and M. Molls, “Definition of Target Volume and Organs at Risk. Biological Target Volume BT - New Technologies in Radiation Oncology,” W. Schlegel, T. Bortfeld, and A.-L. Grosu, Eds. Berlin, Heidelberg: Springer Berlin Heidelberg, 2006, pp. 167–177.

[4] W. D. Bidgood Jr, S. C. Horii, F. W. Prior, and D. E. Van Syckle, “Understanding and using DICOM, the data interchange standard for biomedical imaging,” *J. Am. Med. Inform. Assoc.*, vol. 4, no. 3, pp. 199–212, 1997.

[5] N. Abolhassani, R. Patel, and M. Moallem, “Needle insertion into soft tissue: a survey.,” *Med. Eng. Phys.*, vol. 29, no. 4, pp. 413–431, May 2007.

[6] L. Maier-Hein *et al.*, “Computer-Assisted Needle Insertion for Abdominal Interventions BT - World Congress on Medical Physics and Biomedical Engineering, September 7 - 12, 2009, Munich, Germany,” 2009, pp. 159–162.

[7] M. Maybody, C. Stevenson, and S. B. Solomon, “Overview of navigation systems in image-guided interventions,” *Tech. Vasc. Interv. Radiol.*, vol. 16, no. 3, pp. 136–143, 2013.

[8] L. P. Beyer and P. Wiggermann, “Planning and guidance: New tools to enhance the human skills in interventional oncology,” *Diagn. Interv. Imaging*, vol. 98, no. 9, pp. 583–588, 2017.

[9] J. Kettenbach and G. Kronreif, “Robotic systems for percutaneous needle-guided interventions.,” *Minim. invasive Ther. allied Technol. MITAT Off. J. Soc. Minim. Invasive Ther.*, vol. 24, no. 1, pp. 45–53, Feb. 2015.

[10] S. Hodel, C. Laux, J. Farei-Campagna, T. Götschi, B. Bode-Lesniewska, and D. A. Müller, “The impact of biopsy sampling errors and the quality of surgical margins on local recurrence and survival in chondrosarcoma,” *Cancer Manag. Res.*, vol. 10, pp. 3765–3771, 2018.

[11] N. Hata *et al.*, “Body-mounted robotic instrument guide for image-guided cryotherapy

of renal cancer," *Med. Phys.*, vol. 43, no. 2, pp. 843–853, 2016.

[12] D. Ganguly, S. Chakraborty, M. Balitanas, and T. Kim, "Medical Imaging: A Review BT - Security-Enriched Urban Computing and Smart Grid," 2010, pp. 504–516.

[13] T. M. Deserno, "Fundamentals of Medical Image Processing BT - Springer Handbook of Medical Technology," R. Kramme, K.-P. Hoffmann, and R. S. Pozos, Eds. Berlin, Heidelberg: Springer Berlin Heidelberg, 2011, pp. 1139–1165.

[14] S. Naseera, G. K. Rajini, B. Venkateswarlu, and M. Jasmin Pemeena Priyadarisini, "A review on image processing applications in medical field," *Res. J. Pharm. Technol.*, vol. 10, no. 10, pp. 3456–3460, 2017.

[15] H. Kasban, M. El-bendary, and D. Salama, "A Comparative Study of Medical Imaging Techniques," *Int. J. Inf. Sci. Intell. Syst.*, vol. 4, pp. 37–58, Apr. 2015.

[16] S. Jaiswal, "Applications And Comparison of Medical Imaging Modalities," *Int. J. Eng. Sci. Invent.*, vol. 7, no. 1, pp. 94–100, 2018.

[17] K. Swaraja, "SURVEY ON MEDICAL IMAGE MODALITIES," vol. 2, no. 22, pp. 13–18, 2017.

[18] S. Y. Nam, L. M. Ricles, L. J. Suggs, and S. Y. Emelianov, "Imaging strategies for tissue engineering applications," *Tissue Eng. Part B. Rev.*, vol. 21, no. 1, pp. 88–102, Feb. 2015.

[19] A. Elnakib, G. Gimel'farb, J. Suri, and A. El-Baz, "Medical Image Segmentation: A Brief Survey," in *Multi Modality State-of-the-Art Medical Image Segmentation and Registration Methodologies*, 2011, pp. 1–39.

[20] J. B. A. Maintz and M. A. Viergever, "An Overview of Medical Image Registration Methods," pp. 1–22.

[21] F. Kral, E. J. Puschban, H. Riechelmann, and W. Freysinger, "Comparison of optical and electromagnetic tracking for navigated lateral skull base surgery.," *Int. J. Med. Robot.*, vol. 9, no. 2, pp. 247–252, Jun. 2013.

[22] J. Czajkowska, B. Pyciński, J. Juszczyk, and E. Pietka, "Biopsy needle tracking technique in US images," *Comput. Med. Imaging Graph.*, vol. 65, pp. 93–101, 2018.

[23] A. Veltri, I. Bargellini, L. Giorgi, P. A. M. S. Almeida, and O. Akhan, "CIRSE Guidelines on Percutaneous Needle Biopsy (PNB)," *Cardiovasc. Intervent. Radiol.*, vol. 40, no. 10, pp. 1501–1513, 2017.

[24] S. R. Z. Abdel-Misih and M. Bloomston, “Liver anatomy,” *Surg. Clin. North Am.*, vol. 90, no. 4, pp. 643–653, Aug. 2010.

[25] D. C. Rockey, S. H. Caldwell, Z. D. Goodman, R. C. Nelson, and A. D. Smith, “Liver biopsy,” *Hepatology*, vol. 49, no. 3, pp. 1017–1044, 2009.

[26] S. Ravindran, S. H. Hancox, and D. C. Howlett, “Liver biopsy: Past, present and future,” *Br. J. Hosp. Med.*, vol. 77, no. 2, pp. 90–95, 2016.

[27] S. Albhaisi and A. Sanyal, “Liver Biopsy,” 2019.

[28] “Placement of Liver Biopsy Needle.” [Online]. Available: https://www.healthlinkbc.ca/health-topics/tp13127.

[29] G. P. Coral, A. D. P. Antunes, A. P. A. Serafini, F. B. Araujo, and A. A. de Mattos, “LIVER BIOPSY: IMPORTANCE OF SPECIMEN SIZE IN THE DIAGNOSIS AND STAGING OF CHRONIC VIRAL HEPATITIS,” *Rev. Inst. Med. Trop. Sao Paulo*, vol. 58, p. 10, 2016.

[30] “Human Liver Anatomy.” [Online]. Available: https://netrf.org/for-patients/nets-info/net-treatment/interventional-radiology/.

[31] S. Y. Chuah, “Liver biopsy--past, present and future.,” *Singapore Med. J.*, vol. 37, no. 1, pp. 86–90, Feb. 1996.

[32] A. Boyd, O. Cain, A. Chauhan, and G. J. Webb, “Medical liver biopsy: , indications, procedure and histopathology,” *Frontline Gastroenterol.*, vol. 11, no. 1, pp. 40–47, 2020.

[33] D. Subar, A. Khan, and D. OReilly, “Complications of Liver Biopsy,” in *Liver Biopsy*, InTech, 2011.

[34] R. S. Arellano, M. Maher, D. A. Gervais, P. F. Hahn, and P. R. Mueller, “The difficult biopsy: let’s make it easier.,” *Curr. Probl. Diagn. Radiol.*, vol. 32, no. 5, pp. 218–226, 2003.

[35] A. Regev *et al.*, “Sampling error and intraobserver variation in liver biopsy in patients with chronic HCV infection,” *Am. J. Gastroenterol.*, vol. 97, no. 10, pp. 2614–2618, 2002.

[36] R. D. Odze and J. R. Goldblum, *Surgical Pathology of the GI Tract, Liver, Biliary Tract and Pancreas E-Book*. Elsevier Health Sciences, 2009.

[37] L. Maier-Hein *et al.*, “Human vs. robot operator error in a needle-based navigation

system for percutaneous liver interventions," *SPIE*, vol. 7261, Feb. 2009.

[38] A. Forner *et al.*, "Diagnosis of hepatic nodules 20 mm or smaller in cirrhosis: Prospective validation of the noninvasive diagnostic criteria for hepatocellular carcinoma.," *Hepatology*, vol. 47, no. 1, pp. 97–104, Jan. 2008.

[39] T. L. de Jong, N. J. van de Berg, L. Tas, A. Moelker, J. Dankelman, and J. J. van den Dobbelsteen, "Needle placement errors: do we need steerable needles in interventional radiology?," *Med. Devices (Auckl).*, vol. 11, pp. 259–265, Aug. 2018.

[40] "MPIBC." [Online]. Available: https://www.mpg.de/12018905/frahm-european-inventor-award.

[41] P. J. Keall *et al.*, "The management of respiratory motion in radiation oncology report of AAPM Task Group 76," *Med. Phys.*, vol. 33, no. 10, pp. 3874–3900, 2006.

[42] B. Bussels *et al.*, "Respiration-induced movement of the upper abdominal organs: A pitfall for the three-dimensional conformal radiation treatment of pancreatic cancer," *Radiother. Oncol.*, vol. 68, no. 1, pp. 69–74, 2003.

[43] S. C. Davies, A. L. Hill, R. B. Holmes, M. Halliwell, and P. C. Jackson, "Ultrasound quantitation of respiratory organ motion in the upper abdomen," *Br. J. Radiol.*, vol. 67, no. 803, pp. 1096–1102, 1994.

[44] I. Suramo, M. Paivansalo, and V. Myllyla, "Cranio-caudal movements of the liver, pancreas and kidneys in respiration," *Acta Radiol. - Ser. Diagnosis*, vol. 25, no. 2, pp. 129–131, 1984.

[45] A. Kirilova *et al.*, "Three-Dimensional Motion of Liver Tumors Using Cine-Magnetic Resonance Imaging," *Int. J. Radiat. Oncol. Biol. Phys.*, vol. 71, no. 4, pp. 1189–1195, 2008.

[46] M. C. Mammel and S. E. Courtney, "22 - High-Frequency Ventilation," J. P. Goldsmith, E. H. Karotkin, M. Keszler, and G. K. B. T.-A. V. of the N. (Sixth E. Suresh, Eds. Elsevier, 2017, pp. 211-228.e4.

[47] T. S. D. Murthy and G. Sadashivappa, "Brain tumor segmentation using thresholding, morphological operations and extraction of features of tumor," in *2014 International Conference on Advances in Electronics Computers and Communications*, 2014, pp. 1–6.

[48] B. Devkota, A. Alsadoon, P. W. C. Prasad, A. K. Singh, and A. Elchouemi, "Image

Segmentation for Early Stage Brain Tumor Detection using Mathematical Morphological Reconstruction," *Procedia Comput. Sci.*, vol. 125, pp. 115–123, 2018.

[49] P. G. Rajan and C. Sundar, "Brain Tumor Detection and Segmentation by Intensity Adjustment.," *J. Med. Syst.*, vol. 43, no. 8, p. 282, Jul. 2019.

[50] M. G. Linguraru *et al.*, "Tumor burden analysis on computed tomography by automated liver and tumor segmentation," *IEEE Trans. Med. Imaging*, vol. 31, no. 10, pp. 1965–1976, Oct. 2012.

[51] X. Wu, J. Li, C. Wang, G. Zhang, N. Zheng, and X. Wang, "Application of Different Imaging Methods in the Early Diagnosis of Primary Hepatic Carcinoma," *Gastroenterol. Res. Pract.*, vol. 2016, p. 8763205, 2016.

[52] S. Tang, Y. Chen, R. Xu, Y. Wang, S. Morikawa, and Y. Kurumi, "MR-CT Image Registration in Liver Cancer Treatment with an Open Configuration MR Scanner BT - Biomedical Image Registration," 2006, pp. 289–296.

[53] H. M. Luu, C. Klink, W. Niessen, A. Moelker, and T. van Walsum, "Non-Rigid Registration of Liver CT Images for CT-Guided Ablation of Liver Tumors.," *PLoS One*, vol. 11, no. 9, p. e0161600, 2016.

[54] Li and Zhu, "Application of Image Fusion in Diagnosis and Treatment of Liver Cancer," *Appl. Sci.*, vol. 10, p. 1171, Feb. 2020.

[55] T. Oliveira-Santos *et al.*, "A navigation system for percutaneous needle interventions based on PET/CT images: Design, workflow and error analysis of soft tissue and bone punctures," *Comput. Aided Surg.*, vol. 16, no. 5, pp. 203–219, 2011.

[56] J. Engstrand, G. Toporek, P. Harbut, E. Jonas, H. Nilsson, and J. Freedman, "Stereotactic CT-guided percutaneous microwave ablation of liver tumors with the use of high-frequency jet ventilation: An accuracy and procedural safety study," *Am. J. Roentgenol.*, vol. 208, no. 1, pp. 193–200, 2017.

[57] C. Y. An, J. H. Syu, C. S. Tseng, and C.-J. Chang, "An Ultrasound Imaging-Guided Robotic HIFU Ablation Experimental System and Accuracy Evaluations," *Appl. Bionics Biomech.*, vol. 2017, p. 5868695, 2017.

[58] A. Yamada, J. Tokuda, S. Naka, K. Murakami, T. Tani, and S. Morikawa, "Magnetic Resonance and Ultrasound Image-guided Navigation System using a Needle Manipulator," *Med Phys*, vol. 47, no. 3, pp. 850–858, 2020.

[59] L. Moncharmont, A. Moreau-Gaudry, M. Medici, and I. Bricault, “Phantom evaluation of a navigation system for out-of-plane CT-guided puncture,” *Diagn Interv Imaging*, vol. 96, p. 531, 2015.

[60] P. Durand *et al.*, “Computer assisted electromagnetic navigation improves accuracy in computed tomography guided interventions: A prospective randomized clinical trial,” *PLoS One*, vol. 12, no. 3, pp. 1–19, 2017.

[61] S. Volpi, G. Tsoumakidou, A. Loriaud, A. Hocquelet, R. Duran, and A. Denys, “Electromagnetic navigation system combined with High-Frequency-Jet-Ventilation for CT-guided hepatic ablation of small US-Undetectable and difficult to access lesions,” *Int. J. Hyperth.*, vol. 36, no. 1, pp. 1051–1057, 2019.

[62] D. Putzer *et al.*, “Comparison of Two Electromagnetic Navigation Systems for CT-Guided Punctures: A Phantom Study,” *RoFo Fortschritte auf dem Gebiet der Rontgenstrahlen und der Bildgeb. Verfahren*, vol. 188, no. 5, pp. 470–478, 2016.

[63] D. Xiao *et al.*, “In vivo comparison of two navigation systems for abdominal percutaneous needle intervention,” *Abdom. Radiol.*, vol. 42, no. 7, pp. 1993–2000, 2017.

[64] N. Hungr, I. Bricault, P. Cinquin, and C. Fouard, “Design and Validation of a CT- and MRI-Guided Robot for Percutaneous Needle Procedures,” *IEEE Trans. Robot.*, vol. 32, no. 4, pp. 973–987, 2016.

[65] G. Li *et al.*, “Body-mounted robotic assistant for MRI-guided low back pain injection,” *Int. J. Comput. Assist. Radiol. Surg.*, 2019.

[66] A. Mokry *et al.*, “Evaluation of a novel, patient-mounted system for CT-guided needle navigation—an ex vivo study,” *Neuroradiology*, vol. 61, no. 1, pp. 55–61, 2019.

[67] B. J. Abdullah, C. H. Yeong, and K. L. Goh, “Robotic-assisted thermal ablation of liver tumours,” *Eur Radiol*, vol. 25, p. 246, 2015.

[68] T. Hiraki, T. Kamegawa, T. Matsuno, T. Komaki, J. Sakurai, and S. Kanazawa, “Zerobot®: A remote-controlled robot for needle insertion in CT-guided interventional radiology developed at Okayama University,” *Acta Med. Okayama*, vol. 72, no. 6, pp. 539–546, 2018.

[69] H. J. Won, N. Kim, G. B. Kim, J. B. Seo, and H. Kim, “Validation of a CT-guided intervention robot for biopsy and radiofrequency ablation: Experimental study with an

abdominal phantom," *Diagnostic Interv. Radiol.*, vol. 23, no. 3, pp. 233–237, 2017.

[70] M. Moche *et al.*, "Navigated MRI-guided liver biopsies in a closed-bore scanner: experience in 52 patients," *Eur. Radiol.*, vol. 26, no. 8, pp. 2462–2470, 2016.

[71] B. Treepong, N. Tanaiutchawoot, C. Wiratkapun, and J. Suthakorn, "On the design and development of a breast biopsy navigation system: Path generation algorithm and system with its GUI evaluation," *2014 IEEE-EMBS Int. Conf. Biomed. Heal. Informatics, BHI 2014*, pp. 273–276, 2014.

[72] E. Ben-David, M. Shochat, I. Roth, I. Nissenbaum, J. Sosna, and S. N. Goldberg, "Evaluation of a CT-Guided Robotic System for Precise Percutaneous Needle Insertion," *J. Vasc. Interv. Radiol.*, vol. 29, no. 10, pp. 1440–1446, 2018.

[73] M. Anzidei *et al.*, "Preliminary clinical experience with a dedicated interventional robotic system for CT-guided biopsies of lung lesions: a comparison with the conventional manual technique," *Eur. Radiol.*, vol. 25, no. 5, pp. 1310–1316, 2015.

[74] S. Lim *et al.*, "Robotically assisted long bone biopsy under MRI: cadaver study results," *Int. J. Comput. Assist. Radiol. Surg.*, vol. 14, no. 1, pp. 147–156, 2019.

[75] C. B. Sherman, "Utilization and Accuracy of Biopsy in Patients with Hepatocellular Carcinoma in a Community based Setting," *J. Clin. Gastroenterol. Treat.*, vol. 2, no. 2, pp. 2–5, 2016.

[76] N. Hata *et al.*, "Body-mounted robotic instrument guide for image-guided cryotherapy of renal cancer," *Med. Phys.*, vol. 43, no. 2, pp. 843–853, 2016.

[77] S. A. Yoganathan, K. J. Maria Das, A. Agarwal, and S. Kumar, "Magnitude, Impact, and Management of Respiration-induced Target Motion in Radiotherapy Treatment: A Comprehensive Review," *J. Med. Phys.*, vol. 42, no. 3, pp. 101–115, 2017.

[78] J. Y. Chang *et al.*, "Image–Guided Radiation Therapy for Non–small Cell Lung Cancer," *J. Thorac. Oncol.*, vol. 3, no. 2, pp. 177–186, 2008.

[79] M. A. Clifford, F. Banovac, E. Levy, and K. Cleary, "Assessment of hepatic motion secondary to respiration for computer assisted interventions.," *Comput. aided Surg. Off. J. Int. Soc. Comput. Aided Surg.*, vol. 7, no. 5, pp. 291–299, 2002.

[80] T. Rohlfing, C. Maurer, W. O'Dell, and J. Zhong, "Modeling liver motion and deformation during the respiratory cycle using intensity-based free-form registration of gated MR images," *Proc SPIE*, vol. 4319, May 2001.

[81] H. W. Korin, R. L. Ehman, S. J. Riederer, J. P. Felmlee, and R. C. Grimm, “Respiratory kinematics of the upper abdominal organs: A quantitative study,” *Magn. Reson. Med.*, vol. 23, no. 1, pp. 172–178, 1992.

[82] M. Xi, M.-Z. Liu, Q.-Q. Li, L. Cai, L. Zhang, and Y.-H. Hu, “[Analysis of abdominal organ motion using four-dimensional CT],” *Ai Zheng*, vol. 28, pp. 989–993, Oct. 2009.

[83] J. L. Hallman, S. Mori, G. C. Sharp, H. M. Lu, T. S. Hong, and G. T. Y. Chen, “A four-dimensional computed tomography analysis of multiorgan abdominal motion,” *Int. J. Radiat. Oncol. Biol. Phys.*, vol. 83, no. 1, pp. 435–441, 2012.

[84] R. S. L. Petrusca, P. Cattin, V. De Luca, F. Preiswerk, Z. Celicanin, V. Auboiroux, M. Viallon, P. Arnold, F. Santini, S. Terraz, K. Scheffler, C. D. Becker, “Hybrid Ultrasound/Magnetic Resonance Simultaneous Acquisition and Image Fusion for Motion Monitoring in the Upper Abdomen,” *Invest. Radiol.*, vol. 48, 2013.

[85] C. T. V. De Luca, M. Tschannen, G. Szkely, “A Learning-based Approach for Fast and Robust Vessel Tracking in Long Ultrasound Sequences,” *Med. Image Comput. Comput. Interv.*, vol. LNCS 8149, 2013.

[86] “3Dircadb.” [Online]. Available: https://www.ircad.fr/research/3dircadb/.

[87] I. Wolf *et al.*, “The Medical Imaging Interaction Toolkit (MITK) - a toolkit facilitating the creation of interactive software by extending VTK and ITK,” *Proc SPIE*, May 2004.

[88] “The Architecture of MITK.” [Online]. Available: http://docs.mitk.org/nightly/Architecture.html.

[89] S. Saini and K. Arora, “A Study Analysis on the Different Image Segmentation Techniques,” *Int. J. Inf. Comput. Technol.*, vol. 4, no. 14, pp. 1445–1452, 2014.

[90] S. Yuheng and Y. Hao, “Image Segmentation Algorithms Overview,” vol. 1, 2017.

[91] Y. X. Dong, “Review of Otsu Segmentation Algorithm,” *Adv. Mater. Res.*, vol. 989–994, pp. 1959–1961, 2014.

[92] L. Lo Presti and M. La Cascia, “Multi-modal medical image registration by local affine transformations,” *ICPRAM 2018 - Proc. 7th Int. Conf. Pattern Recognit. Appl. Methods*, vol. 2018-Janua, no. Icpram, pp. 534–540, 2018.

[93] H. Chen, “Mutual Information: A Similarity Measure for Intensity Based Image Registration BT - Advanced Image Processing Techniques for Remotely Sensed Hyperspectral Data,” P. K. Varshney and M. K. Arora, Eds. Berlin, Heidelberg:

Springer Berlin Heidelberg, 2004, pp. 89–108.

[94] H. Grabner, M. Grabner, and H. Bischof, *Real-Time Tracking via On-line Boosting*, vol. 1. 2006.

[95] B. Babenko, M.-H. Yang, and S. Belongie, *Visual tracking with online Multiple Instance Learning*. 2009.

[96] F. Henriques, R. Caseiro, P. Martins, and J. Batista, "High-Speed Tracking with Kernelized Correlation Filters," vol. 37, no. 3, pp. 583–596, 2015.

[97] Z. Kalal, K. Mikolajczyk, and J. Matas, "Tracking-Learning-Detection," *IEEE Trans. Pattern Anal. Mach. Intell.*, vol. 34, no. 7, pp. 1409–1422, 2012.

[98] Z. Kalal, K. Mikolajczyk, and J. Matas, "Forward-backward error: Automatic detection of tracking failures," *Proc. - Int. Conf. Pattern Recognit.*, pp. 2756–2759, 2010.

[99] D. S. Bolme, J. R. Beveridge, and B. A. Draper, "Visual Object Tracking using Adaptive Correlation Filters."

[100] L. Cehovin, "Discriminative Correlation Filter Tracker with Channel and Spatial Reliability."

[101] B. J. Fisher, L. C. Daugherty, and J. E. Reiff, "Planning Target Volume (PTV) BT - Encyclopedia of Radiation Oncology," L. W. Brady and T. E. Yaeger, Eds. Berlin, Heidelberg: Springer Berlin Heidelberg, 2013, pp. 624–625.

نظام محوسب لأخذ عينات خزعة الكبد بالاعتماد على حركة الأعضاء الداخلية وصور الموجات فوق الصوتية

إعداد: ليلى أحمد عمر عباسي

إشراف: د. رضوان قصراوي

الملخص

يعد استخدام الإبر في التشخيص والعلاج من الطرق المهمة والحديثة في الإجراءات السريرية، مثل الحقن، والخزعات التشخيصية، وعلاجات السرطان. ومن أهم استخدامات تقنية الإبر هو أخذ عينات الخزعة من الأعضاء المصابة من أجل التشخيص. إلا أن هناك عوامل كثيرة تحد من الدقة في استخدام الإبر في أخذ العينات مما يزيد من نسبة الأخطاء في التشخيص.

يتيح التقدم في التكنولوجيا الطبية وتطوير الأنظمة المحوسبة المعتمدة على الصور الطبية دقة وفعالية أعلى في استخدام الإبر في التشخيص والعلاج. على الرغم من توفر العديد من الأنظمة المحوسبة وأساليب التصوير الطبي المتقدمة، إلا أنه ما زال يوجد أخطاء في تطبيقات استخدام الإبر في العلاج والتشخيص، كما أن هذه الأنظمة عالية التكلفة ولا تعالج كافة العوامل المسببة لهذه الأخطاء وما زالت في مراحل تجريبية ولم يتم تطبيقها في العيادات.

ناقشت الدراسات السابقة التأثير الرئيسي للتنفس على حركة الأعضاء، وعرضت التأثير الكبير للتنفس على حركة الأعضاء، وأكدت على حركة العضو كمصدر رئيسي لخطأ استهداف المنطقة في الإجراءات التداخلية. على الرغم من ذلك لا تتعامل الأنظمة المحوسبة لهذه الإجراءات مع عامل الحركة نتيجة للتنفس بطريقة فعالة وعملية للسيطرة عليه. استكمالا للتطور التكنولوجي للأنظمة المحوسبة، يقدم هذا البحث نظام محسوب موجه بالصور الطبية والذي يأخذ بعين الاعتبار حركة الأعضاء نتيجة التنفس، ومدمج مع معالجة الصور الطبية وتقنيات الرؤية الحاسوبية في هذه الأطروحة، بهدف التحكم في مصادر الخطأ في وضع الإبرة في الإجراءات التداخلية لأخذ عينات الخزعة في عملية تتماشى مع سيرعمل العيادة الحالي. يوفر النظام للأطباء أدوات لتحديد خطة أخذ خزعة خاصة بالمريض، وتتبع الهدف أثناء الإجراء الطبي، إدخال وإستخراج الإبرة مع مراعاة حركة الأعضاء الداخلية وتتبعها من خلال تقنيات تحليل الصور.

نفذ النظام خوارزمية MOSSE لتتبع المنطقة المستهدفة أثناء الإجراء، وتم تقييمه على عينة من الصور طبية ل 9 مرضى من خلال 27 إجراء محاكاة لأخذ عينات من ورم الكبد، وأظهر تتبعًا موثوقًا مع دقة عالية للنظام مع متوسط الخطأ الكلي 1.78 ± 0.8 ملم. تبين أن الحركة الداخلية للأعضاء عامل مهم ومسبب رئيسي للأخطاء وإهماله قد يزيد من أخطاء التشخيص في إجراءات أخذ الخزع. وجود نظام محوسب يسيطر على إدخال الإبرة بحسب تتبع حركة الأعضاء الداخلية ساهم بتقليل الأخطاء وفتح الأفاق لتقديم حلول طبية محوسبة حرجة.